Equilibrium Fractionation of Non-traditional Isotopes: a Molecular Modeling Perspective

Marc Blanchard, Etienne Balan, Edwin A Schauble

Equilibrium fractionation of non-traditional isotopes: A molecular modeling perspective

Marc Blanchard, Etienne Balan

Institut de Minéralogie, de Physique des Matériaux, et de Cosmochimie (IMPMC), Sorbonne Universités, UPMC Univ Paris 06, UMR CNRS 7590, Muséum National d'Histoire Naturelle, UMR IRD 206, 4 place Jussieu, F-75005 Paris, France

Edwin A. Schauble

Department of Earth, Planetary and Space Sciences
University of California, Los Angeles
Los Angeles, California 90095-1567, U.S.A.

INTRODUCTION

The isotopic compositions of natural materials are determined by their parent reservoirs, on the one hand, and by fractionation mechanisms, on the other hand. Under the right conditions, fractionation represents isotope partitioning at thermodynamic equilibrium. In this case, the isotopic equilibrium constant depends on temperature, and reflects the slight change of free energy between two phases when they contain different isotopes of the same chemical element. The practical foundation of the theory of mass-dependent stable isotope fractionation dates back to the mid-twentieth century, when Bigeleisen and Mayer (1947) and Urey (1947) proposed a formalism that takes advantage of the Teller-Redlich product rule (Redlich 1935) to simplify the estimation of equilibrium isotope fractionations. In this chapter, we first give a brief introduction to this isotope fractionation theory. We see in particular how the various expressions of the fractionation factors are derived from the thermodynamic properties of harmonically vibrating molecules, a surprisingly effective mathematical approximation to real molecular behavior. The central input data of these expressions are vibrational frequencies, but an approximate formula that requires only force constants acting on the element of interest can be applied to many non-traditional isotopic systems, especially at elevated temperatures. This force-constant based approach can be particularly convenient to use in concert with first-principles electronic structure models of vibrating crystal structures and aqueous solutions. Collectively, these expressions allow us to discuss the crystal chemical parameters governing the equilibrium stable isotope fractionation.

Since the previous volume of Reviews in Mineralogy and Geochemistry dedicated to non-traditional stable isotopes, the number of first-principles molecular modeling studies applied to geosciences in general and to isotopic fractionation in particular, has significantly increased. After a concise introduction to computational methods based on quantum mechanics, we will focus on the modeling of isotopic properties in liquids, which represents a bigger methodological challenge than small molecules in gas phase, or even minerals. Our ability to produce reliable theoretical mineral-solution isotopic fractionation factors is essential for many geosciences problems. The main modeling approaches used in recent studies of fractionation in

liquids are molecular cluster models and molecular dynamics with periodic boundary conditions. Their relative advantages and drawbacks will be discussed. So far, the vast majority of theoretical studies applied to isotopic fractionation have been based on the harmonic approximation; in most cases anharmonic effects will be smaller than uncertainties associated with other imperfections in the models (especially in calculated vibrational frequencies), but in some cases (e.g., liquid phases with light elements) it will be important to be able to go beyond the harmonic approximation. More sophisticated methods, such as thermodynamic integration coupled to path integral molecular dynamics, can account for anharmonic effects as well as quantum nuclear effects. We will introduce the basic concepts of this technique and will give some examples of their application.

Among the non-traditional isotopes, the iron isotope system has probably developed the richest and most methodologically varied theoretical literature. This is partly due to the fact that isotope fractionation factors of Mössbauer-active elements (including iron, via ^{57}Fe) can be independently determined using Mössbauer spectroscopy and nuclear resonant inelastic X-ray scattering, which are closely related techniques that probe the vibrational properties of the target element. Expressions used to derive fractionation factors from these spectroscopic techniques are introduced, the accuracy of each method will be discussed, and the results are compared with first-principles calculations.

The discovery of mass-independent isotope fractionation of non-traditional stable isotope systems including Hg, Tl, and U over the past decade has expanded the scope of "stable" isotope geochemistry to include a long-lived radioactive element and almost the whole range of naturally occurring atomic numbers. It has also created a need for theoretical studies of new fractionation mechanisms. Nuclear field shift effects, first proposed to explain laboratory isotope enrichment experiments, including uranium, are now thought to play an important role in driving natural fractionation in uranium and thallium, and a secondary role in mercury isotope geochemistry. Large photochemically induced mass-independent fractionation effects in the mercury isotope system are yet to be explained beyond a qualitative level, and remain an important challenge for isotope fractionation theory. In light isotope systems (particularly ^{16}O-^{17}O-^{18}O) it is now possible to measure variability of mass dependence for different types of fractionation, ranging from equilibrium partitioning to kinetic fractionation. The potential for using variations in mass dependence to identify the types of fractionation affecting non-traditional elements is also a topic of emerging interest for theoretical studies.

THEORETICAL FRAMEWORK

Equilibrium fractionation theory

This section is largely inspired by the articles of Bigeleisen and Mayer (1947), and Ishida (2002).

Let's consider an isotopic exchange reaction between two molecules A and B, involving a single atomic position:

$$AX' + BX \leftrightarrows AX + BX' \qquad (1)$$

The prime symbol refers to the light isotope of the element X. As with any chemical reaction, the equilibrium constant, K_{eq}, can be determined from the free energies of the

reactants and products. Isotopic exchange reactions do not, in general, involve significant pressure-volume work because the number of molecules on both sides of the reaction is the same, and because isotope substitution has a negligible effect on the molar volumes of the phases under normal conditions. The above assumption is not true for a complete substitution of hydrogen by deuterium, for instance, or for certain solid-gas equilibria (e.g., Jancso et al. 1993; Horita et al. 2002). Under these general conditions, the standard Gibbs free energy of the exchange reaction can be related to the difference in the Helmholtz free energy of the pure isotopomers (AX', AX, BX' and BX):

$$\Delta F = F(AX) + F(BX') - F(AX') - F(BX)$$

The Helmholtz free energy is related to the molecular partition function, *Q by*:

$$F = - \mathrm{N_a k} T \ln(Q/\mathrm{N_a})$$

where k is Boltzmann's constant, $\mathrm{N_a}$ the Avogadro number, and T is the absolute temperature. It is thus possible to express the equilibrium constant of the exchange reaction as:

$$K_{eq} = \frac{Q(AX) \times Q(BX')}{Q(AX') \times Q(BX)} \qquad (2)$$

The molecular partition function is given by the following expression:

$$Q = \sum_n \exp(-E_n / \mathrm{k}T)$$

where the sum spans all the quantum states of the molecule, referred to by their index n and their corresponding energies E_n.

A classical partition function, Q_{cl} can be obtained by integration over continuous momenta and position variables that relate to the kinetic energy and potential energy of the molecule, respectively. Its expression is also a function of the symmetry number of the molecule (i.e. the number of equivalent ways to orient a molecule in space); see equation (5) of Bigeleisen and Mayer (1947). Importantly, atomic masses are only involved in the definition of the kinetic energy term; whereas the configurational integral, obtained from the potential energy of the system, is assumed to be mass-independent. Considering the ratio of the partition functions of the two isotopically substituted molecules, the configurational integrals and the contribution arising for atoms other than the exchanged isotopes cancel out, leading to the following expression:

$$\left(\frac{Q}{Q'}\right)_{cl} = \frac{s'}{s}\left(\frac{m}{m'}\right)^{3/2}$$

where s is the symmetry number and m, the atomic mass of isotopes. By inserting this expression into Equation (2), the atomic masses cancel out and one obtains the classical value of the equilibrium constant:

$$(K_{eq})_{cl} = \frac{s_{AX'}}{s_{AX}} \frac{s_{BX}}{s_{BX'}} \qquad (3)$$

This ratio of symmetry numbers will not lead to an isotopic fractionation as it merely represents the relative probabilities of forming symmetric and antisymmetric molecules. This corresponds to a perfectly random distribution of isotopes; a situation found at T =

∞. This demonstrates that isotopic fractionation is a purely quantum effect that cannot be explained by classical statistical mechanics.

The harmonic quantum molecular partition function of a molecule in gas phase, can be written as a product of translational, rotational, vibrational and electronic partition functions:

$$Q_{qm} = \left(Q_T\right)_{qm} \times \left(Q_R\right)_{qm} \times \left(Q_V\right)_{qm} \times \left(Q_E\right)_{qm}$$

The electronic structure of a molecule is usually assumed to be isotope-independent, so the electronic term is neglected. In some cases, isotope effects will have measurable electronic contributions: isotope mass shift, nuclear field shift effect and nuclear spin effect (e.g. Bigeleisen 1996). Fractionations caused by the nuclear field shift and spin effects will be discussed in a later section. The mass shift arises from the coupling of the motion of the nuclei and the electrons. Mass shift can be important in reaction involving hydrides, i.e. up to a small percentage of H-D fractionation factors (e.g. Kleinman and Wolfsberg 1973), but becomes quickly negligible for heavier atoms since it scales with $\delta M/M^2$. Partition functions for translational and rotational motions are formally quantum mechanical, and sensitive to isotope substitution, but in practice the quanta for both types of motion are so small and closely spaced for most molecules that they do not deviate significantly from their classical equivalents at temperatures relevant to geochemistry (see Schauble 2004, for additional details). This will hold in all cases except hydrogen, where a more sophisticated treatment of rotation may be needed at low temperatures. The classical expressions are not given here since most of their parameters will cancel out in the next step, but they can be found in literature (e.g., Richet et al. 1977; Schauble 2004; Liu et al. 2010). As a result, it is generally the case that only vibrational motions need a quantum-mechanical treatment, and it is vibrational energy that plays the central role in controlling the distribution of isotopes between two phases in thermodynamic equilibrium. The harmonic vibrational partition function is defined by:

$$\left(Q_V\right)_{qm} = \prod_{i=1}^{3N-6} \frac{e^{-\mathrm{h}\nu_i/(2\mathrm{k}T)}}{1-e^{-\mathrm{h}\nu_i/(\mathrm{k}T)}}$$

where h is Planck's constant and ν_i is the frequency of the vibrational mode i. A molecule with N atoms will have $3N$-6 vibrational degrees of freedom (in addition to 3 rotational and 3 translational degrees of freedom) while a linear molecule will have $3N$-5 vibrational degrees of freedom.

As classical contributions to the partition functions only play a bookkeeping role in the isotopic fractionation, it is useful to define a reduced partition function by ratioing the quantum partition function to its classical counterpart (Q_{qm}/Q_{cl}). The ratio of reduced partition function, commonly referred to as β, can be written as:

$$\beta_{AX} = \frac{Q_{qm}(AX)/Q_{cl}(AX)}{Q_{qm}(AX')/Q_{cl}(AX')} \qquad (4)$$

The equilibrium isotope fractionation factor of the exchange reaction (1), i.e. $\alpha_{AX\text{-}BX}$, can thus be expressed as a function of the reduced partition function ratios and is related to the equilibrium constant through the following relation (using Equations (2) and (3)):

$$\alpha_{AX-BX} = \frac{\beta_{AX}}{\beta_{BX}} = \frac{Q_{qm}(AX) \times Q_{qm}(BX')}{Q_{qm}(AX') \times Q_{qm}(BX)} \times \frac{Q_{cl}(AX') \times Q_{cl}(BX)}{Q_{cl}(AX) \times Q_{cl}(BX')}$$

$$= \frac{(K_{eq})_{qm}}{(K_{eq})_{cl}}$$

$$= \frac{s_{AX'}}{s_{AX}} \times \frac{s_{BX}}{s_{BX'}} \times (K_{eq})_{qm}$$

The above relation shows that, when $(K_{eq})_{qm}$ is equal to $(K_{eq})_{cl}$, there will be no isotopic fractionation (i.e. $\alpha_{AX\text{-}BX} = 1$). This situation occurs, for instance, at very high temperatures when isotopes are randomly distributed. Conversions between fractionation factors and equilibrium constant, written here for the simple isotopic exchange reaction (1), can be more complicated, depending on molecular stoichiometry (Schauble 2004; Liu et al. 2010). By analogy with the isotopic fractionation factor α, we can also see the reduced partition function ratio β_{AX} as the isotopic fractionation factor between the substance AX and an ideal atomic gas of X. This formulation is a convenient way to tabulate the theoretical fractionations with a simple point of comparison. Fractionations are typically very small, on the order of parts per thousand for non-traditional stable isotopes, so it is common to use the notation 1000 ln α or 1000 ln β expressing the result in permil (‰). The β-factor being the central quantity of theoretical studies, we report below the expressions that apply to situations commonly encountered (i.e. molecules or condensed phases, complete or site by site isotopic substitution).

By inserting the expressions of the quantum and classical partition functions into Equation (4), we obtain the following expression for a molecule in gas phase having only one exchangeable atom:

$$\beta_{AX} = \left(\frac{m'}{m}\right)^{3/2} \times \left(\frac{M}{M'}\right)^{3/2} \times \left(\frac{I_x I_y I_z}{I'_x I'_y I'_z}\right)^{1/2} \times \left(\prod_{i=1}^{3N-6} \frac{e^{-h\nu_i/(2kT)}}{1-e^{-h\nu_i/(kT)}} \times \frac{1-e^{-h\nu'_i/(kT)}}{e^{-h\nu'_i/(2kT)}}\right) \qquad (5)$$

where M is the mass of molecule AX, M' is the mass of molecule AX', and I_x, I'_x, etc. are the moments of inertia along each cartesian axis.

Alternatively, for a molecule having n exchangeable atoms, the β_{AX} can be determined from the β_i related to a specific atomic site i:

$$\beta_{AX} = \frac{1}{n}\sum_{i=1}^{n}\beta_i = \frac{1}{n}\sum_{i=1}^{n}\frac{Q_{qm}(AX'_{n-1}X_i)}{Q_{qm}(AX'_n)} \times \left(\frac{m'}{m}\right)^{3/2} \qquad (6)$$

In this "site by site" approach, $Q_{qm}(AX'_{n\text{-}1}X_i)$ corresponds to the partition function of the molecule having the atom X' on the site i substituted with X while $Q_{qm}(AX'_n)$ represents the partition function of the molecule with no substituted atoms.

If we further use the Teller-Redlich product rule (e.g., Redlich 1935; Wilson et al. 1955):

$$\left(\frac{I_x I_y I_z}{I'_x I'_y I'_z}\right)^{1/2} \times \left(\frac{M}{M'}\right)^{3/2} \times \left(\frac{m'}{m}\right)^{3N/2} \times \prod_{i=1}^{3N-6}\frac{\nu'_i}{\nu_i} = 1$$

then Equation (5) transforms into a more general expression applicable to any molecule in gas phase undergoing a complete isotopic substitution (i.e. all X' atoms are substituted with X):

$$\beta_{AX} = \left[\prod_{i=1}^{3N-6} \frac{\nu_i}{\nu'_i} \times \frac{e^{-h\nu_i/(2kT)}}{1 - e^{-h\nu_i/(kT)}} \times \frac{1 - e^{-h\nu'_i/(kT)}}{e^{-h\nu'_i/(2kT)}} \right]^{1/n} \quad (7)$$

This more convenient form involving only the vibrational frequencies before and after full isotope substitution, assumes that: (i) the free energy change associated to the isotopic substitution of an atom X does not depend on the isotopic nature of the surrounding X atoms, and (ii) the β-factor of each atomic site weakly depends on the site. These assumptions are generally valid except in some specific cases, like for instance, when deuterium is substituted for hydrogen in a water molecule.

Crystalline materials differ from gaseous molecules by their spatial extension involving the presence of long-range interactions. This implies that their vibrational spectra do not exhibit a finite number of vibrational frequencies but rather correspond to a continuum. In crystals, a vibrational mode is defined by a frequency of vibration, the atomic displacement pattern in a given cell and a wave-vector q that describes the phase relation of the atomic displacements in the other cells of the crystal. The wave-vector is defined in the reciprocal space and belongs to the first Brillouin zone. The vibrational frequency thus depends on the wave-vector. It is possible to build dispersion curves by reporting the frequency along specific directions in the reciprocal space, and vibrational density of states by integration over the whole Brillouin zone. A more detailed description of the crystal vibrational properties applied to isotope fractionation can be found in Young et al. (2015). This feature of crystals can be taken into account by modifying the partition function. The energy differences associated with translation motions cancel at equilibrium and the rotational term disappears in crystals. The partition function, in the harmonic approximation, is thus defined by:

$$Q_{qm} = \left[\prod_{i=1}^{3N} \prod_{\{q\}} \frac{e^{-h\nu_{q,i}/(2kT)}}{1 - e^{-h\nu_{q,i}/(kT)}} \right]^{1/N_q} \quad (8)$$

where $\nu_{q,i}$ is now the frequency of the vibrational mode i, along the wave-vector q. N corresponds to the number of atom in the crystal unit cell. The second product is performed on a uniform grid of N_q q-vectors in the Brillouin zone. In practice, the number of frequencies used is still finite but beyond a sufficiently large number of q-vectors, results are properly converged.

By combining Equations (4) and (8), we obtain the general expression of the reduced partition function ratio (i.e. β-factor) for a crystal undergoing a complete isotopic substitution (i.e. all n atoms X' of the unit-cell are substituted with X):

$$\beta_{AX} = \left(\frac{m'}{m} \right)^{3/2} \times \left[\prod_{i=1}^{3N} \prod_{\{q\}} \frac{e^{-h\nu_{q,i}/(2kT)}}{1 - e^{-h\nu_{q,i}/(kT)}} \times \frac{1 - e^{-h\nu'_{q,i}/(kT)}}{e^{-h\nu'_{q,i}/(2kT)}} \right]^{1/nN_q} \quad (9)$$

Alternatively, Equation (6) for a "site by site" isotopic substitution is still valid for crystals. The rotational and translational terms also disappear from the Teller-Redlich product rule, yielding the high-temperature product rule of Kieffer (1982):

$$\left(\frac{m'}{m}\right)^{3/2} \times \left(\prod_{i=1}^{3N}\prod_{\{q\}}\frac{\nu'_{q,i}}{\nu_{q,i}}\right)^{1/nN_q} = 1$$

This high-temperature product rule imposes the isotope fractionation to be nil at very high-temperatures. If we take advantage of this rule, Equation (9) then becomes:

$$\beta_{AX} = \left[\prod_{i=1}^{3N}\prod_{\{q\}}\frac{\nu_{q,i}}{\nu'_{q,i}} \times \frac{e^{-\mathrm{h}\nu_{q,i}/(2\mathrm{k}T)}}{1-e^{-\mathrm{h}\nu_{q,i}/(\mathrm{k}T)}} \times \frac{1-e^{-\mathrm{h}\nu'_{q,i}/(\mathrm{k}T)}}{e^{-\mathrm{h}\nu'_{q,i}/(2\mathrm{k}T)}}\right]^{1/nN_q} \quad (10)$$

Liquid phases exhibit a higher degree of complexity, in particular because of the absence of long-range translational order and because of their dynamical behavior. More approximations are needed. The isotopic properties of liquid phases can be determined by adopting either the same approach as for crystals (i.e. building a periodic model), or the approach developed for gaseous molecules (i.e. building an isolated molecular cluster of variable size). The latter method can be justified for dissolved molecules that remain more or less intact in solution or for aqueous complexes where intra-complex bonds are probably much stronger than interactions with bulk solvent. The additional complexities that arise in dealing with liquid phases will be discussed in a later section.

Approximate formula based on force constants

The above equations relate conveniently the isotopic fractionation factor to the vibrational frequencies but Bigeleisen and Mayer (1947) also derived a series of approximate formulae that are useful when all vibrational frequencies are not available and also for improving our understanding of the parameters that control equilibrium isotopic fractionation between two phases. Thus, if the frequency shift associated with the isotopic substitution is small and if the reduced energy is small (i.e. hν/kT ≤ 2) then Equations (7) or (10) become:

$$\beta_{AX} = 1 + \sum_i \frac{\mathrm{h}^2\,\Delta\nu_i^2}{24(\mathrm{k}T)^2}$$

Treating the vibrations as harmonic, squared vibrational frequencies can be related to the force constants and masses. By doing so, the reduced partition function ratio can be expressed as a function of the force constants acting on the element of interest:

$$\beta_{AX} = 1 + \frac{m-m'}{m\,m'}\left(\frac{\mathrm{h}}{2\pi}\right)^2 \frac{F}{24(\mathrm{k}T)^2} \quad (11)$$

F is the sum of force constants in three orthogonal directions opposing displacement of the atom X from its equilibrium position. If atoms X are located in more than one crystallographic site, the force constant for all sites must be averaged. The full derivation of the approximate formula (11) from Equations (7) or (10) can be found for instance in Young et al. (2015). This expression is a valid approximation for Equation (10): (i) at relatively high temperature (hν/kT < 2 implies, for instance, a temperature higher than 360 K if the vibrations involving atom X in phase A have wavenumbers, ω=ν/c, smaller than 500 cm^{-1} (1 cm^{-1} is equivalent to 30.0 GHz), or a temperature higher than 720 K if the relevant vibrations extend up to 1000 cm^{-1}), (ii) when the difference in mass between the two isotopes is sufficiently small relative to the average atomic mass (this assumption

excludes the very light elements such as hydrogen), (iii) assuming isotope-independent force constants; it is also worth noting that Equation (11) still assumes a harmonic vibrational partition function.

The expression (11) clearly shows that, under the conditions of validity just mentioned, equilibrium isotopic fractionation varies proportionally to the reciprocal of the square of the temperature. When the reduced energy $h\nu/kT$ becomes much higher than 2 (i.e. at low temperature or for high-frequency vibrations), it can be shown that the temperature dependence of fractionation factor weakens and tends to a $1/T$ behavior. This leads to a concave-down curvature of β-factors when plotted against $1/T^2$ and this curvature is more pronounced as one moves away from the conditions of validity of Equation (11). The mass-dependence of the same equation indicates that isotopic fractionations become smaller for heavy elements. Equation (11) also predicts that, at equilibrium, the heavy isotopes of an element will concentrate in the phase where the force constants are the greatest, i.e. in the phase where the element of interest involves the stiffest bonds (e.g., element in higher oxidation state, with lower coordination number). The two first points, i.e. temperature dependence and mass dependence, are well illustrated by the iron and oxygen β-factors of the goethite (Fig. 1). In this iron oxyhydroxide, vibrations involving iron atoms correspond to wavenumbers smaller than 600 cm^{-1}, which dictates that Equation (11) is valid above ~ 400 K. Even at lower temperatures (i.e. in the stability field of goethite), Figure 1 shows that the departure of this approximate formula from Equation (10) is smaller than 0.5 ‰. Because oxygen is much lighter that iron, the equilibrium isotope fractionation factors are much larger (i.e. oxygen β-factor is ~6 times larger than iron β-factor). In goethite, half oxygen atoms are hydroxylated. The bending and stretching vibrational modes of these OH groups (observed at ~ 800 cm^{-1} and above 3000 cm^{-1}, respectively) contribute to the oxygen β-factor. This explains why, in the case of the hydroxylated oxygen atoms, Equation (11) is not a valid approximation and meets the "correct" β-factor curve only at very high temperature whereas the approximation still holds for the other oxygen atoms.

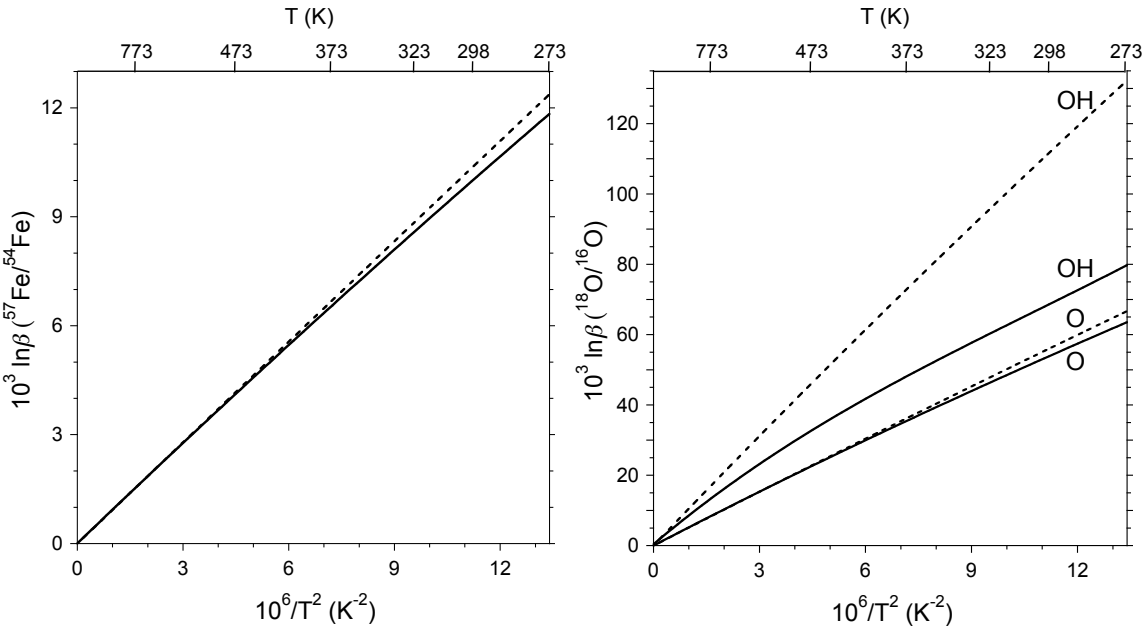

Figure 1. Temperature dependence of the iron (left) and oxygen (right) β-factors of goethite (α-FeOOH). Results obtained using the approximate formula (11) based on force constants (dashed

lines, unpublished data) are compared with the results given by Equation (10) using all vibrational frequencies (solid lines, Blanchard et al. 2015).

In first-principles calculations based on quantum-mechanics, the determination of β-factors using Equations (7) or (10) requires computing all vibrational frequencies, which is computationally expensive, whereas only electronic energy calculations performed for a limited number of positions of the atom of interest in the vicinity of its equilibrium position are needed to apply the approximate formula (11). When the conditions of validity stated above are met, the use of Equation (11) allows consideration of more phases, and phases with greater structural complexity. This includes liquids and crystal defects, which may require large model systems (i.e. more than a hundred of atoms). This approach has been applied for discussing the Cr isotope fractionation in conditions relevant to the differentiation of the Earth's core (Moynier et al. 2011), the Li isotope fractionation between minerals and aqueous solutions at high pressure and temperature (Kowalski and Jahn 2011), and the S isotope fractionation of sulfate groups incorporated in major calcium carbonates (Balan et al. 2014). Without performing first-principles calculations, a qualitative estimation of the fractionation factors between phases where the element of interest involves contrasted bonding schemes, can be obtained by determining the force constants from an ionic model. In this model based on Pauling's rules, the force constant is assessed mainly from the valences and ionic radii of the central element and its first neighbors. A description and application of the method for non-traditional isotopes is presented in Young et al. (2015). This ionic model derives from earlier studies that demonstrated and used the correlation existing between bond types and oxygen isotope fractionation in silicate minerals (e.g., Taylor and Epstein 1962; Garlick 1966; Smyth and Clayton 1988; Schütze 1980; Richter and Hoernes 1988). Even if this type of ionic model does not show a great accuracy, it highlights the basic crystal chemical parameters that govern the equilibrium stable isotope fractionation, by affecting the stiffness of interatomic bonds.

MODELING APPROACHES

Quantum-mechanical molecular modeling

As shown in the previous section, the determination of the equilibrium isotope fractionation factors can be related to the change of vibrational frequencies associated to the isotopic substitution. These vibrational frequencies can be calculated from empirical force fields built using experimental measurements like structural parameters, elastic properties or known vibrational frequencies. A review of these methods can be found in Schauble (2004). The alternative approach that spread out during the last decade thanks to the advances in processor speed and memory size, consists in using quantum-mechanical molecular modeling. We will give here only a short introduction aiming at helping experimental geochemists to approach these theoretical tools but many general or specialized publications are available elsewhere, like for instance in previous Reviews in Mineralogy and Geochemistry volumes (Cygan and Kubicki 2001; Perdew and Ruzsinszky 2010).

The properties of any material can in principle be obtained from the laws of Quantum Mechanics by solving the equations describing the interactions between nuclei and electrons. In practice, a number of approximations are needed to address this complex problem. The first is the Born-Oppenheimer approximation, which considers

that the rapid motion of electrons is decoupled from the slower motion of nuclei. Electronic wavefunctions are obtained by solving the Schrödinger equation for a system to which the positions of the nuclei are fixed external parameters. The energy of the system is then a function of the nuclei positions and the nuclei dynamics can be described by considering their motions on a potential energy surface. In comparison, empirical force fields use analytic functions to approximately describe the potential energy surface in terms of interatomic distance, oxidation state, effective ionic charge, and similar parameters that can be fitted by detailed examination of either experimental data or theoretical calculations. This parameterization of the potential energy surface may be assumed to be transferable, meaning that interatomic interactions in a group of related structures can be calculated using parameters fit to data from only one, or a subset of them. The reliability of empirical force fields will then be highly dependent on the quality of data available for parameter fitting, on the correct choice of structural variables to fit, the correct choice of suitable analytic functional forms, and on the consistency of electronic structure in the group of substances to which the force field is applied. Because of this chain of assumptions, and the use of empirical data, it can be difficult to assess the suitability of an empirical force field for calculating isotope fractionation factors. In addition, spectroscopic-quality force fields are not always available for substances of interest, especially for compounds and molecules containing heavy elements, unusual structures, or less common oxidation states. For these reasons, the information obtained using first-principles calculations is often more straightforward to generate, and easier to test against known vibrational and structural properties, than the outputs of analytic potentials. Against this caution, however, it should be noted that typical force-field parameterizations are much more mathematically efficient than electronic structure calculations, making it possible to probe systems with large numbers of atoms and/or dynamical disorder (such as liquids or trace-element substituted crystals) with relatively modest computational effort.

In the quantum mechanical treatment, the Schrödinger equation of a multiple-electron system is most often solved using one of two different schemes. The Hartree-Fock (HF) method (Roothaan 1951) aims at determining the best multi-electronic wavefunction by combining mono-electronic wavefunctions (the so-called orbitals). The multi-electronic wavefunction exactly obeys the Pauli exclusion principle, whereas Coulombic interactions between different electrons are treated in a mean field approximation. It can be shown that the exact system energy is always lower than the Hartree-Fock energy, the difference being often referred to as the correlation energy. Instead of focusing on wavefunctions, density functional theory (DFT) (Hohenberg and Kohn 1964) is based a theorem requiring that all the ground state properties of a system of electrons moving under the influence of an external potential are uniquely determined by its electron density. Therefore, the ground state energy is a functional of the electronic density. Hohenberg and Kohn (1964) also demonstrated that the ground state energy can be obtained variationally because only the exact ground-state density minimizes this functional. Kohn and Sham (1965) proposed a practical scheme to build this functional by showing that a system of N interacting electrons can be treated as a fictitious system of N electrons that do not interact with each other but operate in an effective external potential taking into account an exchange-correlation term. The corresponding mono-electronic equations, called Kohn-Sham equations, can be solved via an iterative and self-consistent procedure starting from an arbitrary electron density. This procedure should lead to the density that minimizes the energy (i.e. the exact ground state electronic

density). Unfortunately, the exact expression of the exchange-correlation potential is unknown and approximate expressions have to be used. Two commonly used approximations are the local density approximation (LDA, based for example on a homogeneous electron gas) and the generalized gradient approximation (GGA) taking partial account of non-homogeneous effects. DFT is popular in part because it provides a description of the electronic ground state of many systems that is more accurate than standard HF methods, at a similar computational cost (for molecules). In this way, DFT makes it possible to efficiently model the static or dynamic properties of relatively complex systems, such as periodic systems containing up to few hundred atoms per unit cell. Unlike HF-based methods, however, there is not (or at least not yet) a well-defined hierarchy of post-GGA theories that can be used to systematically improve the accuracy of DFT models. Partial corrections for some known shortcomings in standard DFT functionals are well established and effective, such as the "DFT+*U*" technique for improving DFT models of transition-element oxides (Anisimov et al. 1991; Cococcioni and de Gironcoli 2005) or the various methods for including the dispersion interactions into DFT (e.g. Grimme 2011), however.

In practice, electronic wavefunctions are represented using a finite set of fixed functions. These functions can be localized on the atomic positions (as are the atomic orbitals) or can consist of plane waves (which correspond to solutions of the Schrödinger equation for a free particle). Although not a stringent rule, localized basis sets are well suited for isolated molecules or clusters of molecules; whereas plane-waves are more appropriate to treat extended and periodic systems, such as crystalline solids. Localized basis sets make it possible to use hybrid DFT-HF methods such as the Becke three parameter Lee-Yang-Parr (B3LYP) method (Lee et al. 1988; Becke 1993), designed to emphasize the best features of each both theories. Hybrid methods are most commonly used to model the structure and vibrational frequencies of molecules. In order to reduce the computation cost without losing accuracy, it is also possible to restrict the explicit electronic structure calculations to the valence electrons because chemical properties mostly involve changes in the distribution of valence electrons. In this simplified treatment, the potential created by the atomic nucleus and core electrons is replaced by a pseudopotential. Pseudopotentials are most commonly used in conjunction with plane-wave basis sets for elements with $Z > 2$, or in localized basis function calculations involving elements with $Z \gtrsim 20$. Many different types of pseudopotentials have been developed, and high-quality public libraries of basis sets and pseudopotentials for almost all naturally occurring elements are now available online (e.g., GBRV, http://www.physics.rutgers.edu/gbrv/, Garrity et al. 2014; SSSP, http://materialscloud.org/sssp/; EMSL Basis Set Exchange, bse.pnl.gov/bse/portal, Schuchardt et al. 2007). These theoretical methods are implemented in numerous commercial and open-source software packages such as ABINIT (Gonze et al. 2002), CASTEP (Clark et al. 2005), CRYSTAL (Dovesi et al. 2014), GAMESS (Schmidt et al. 1993), Gaussian (Frisch et al. 2009), NWChem (Valiev et al. 2010), Quantum ESPRESSO (Giannozzi et al. 2009), or VASP (Kresse and Furthmüller 1996).

There are typically three steps in first-principles calculations for obtaining the vibrational frequencies needed for the determination of isotope fractionation factors. In the first step, the minimum-energy static structure is determined via geometric relaxation. From an initial guess geometry, often the experimentally determined structure, the forces on each atom and the stress over the cell are calculated, and a refined guess structure is determined. This procedure continues iteratively until the residual forces and stress are

sufficiently small. Once the minimum-energy configuration has been calculated, the second step is the determination of force constants for displacements of the atomic nuclei from their equilibrium positions. Finally, vibrational frequencies are determined by a calculation with model force constants and appropriate isotopic masses (Baroni et al. 2001). Isotope substitution is expected to have a negligible effect on electronic structure, so a matrix of force constants for the common isotope in a molecule or a crystal can be recycled to estimate vibrational frequencies of uncommon isotope-substituted species. This means that frequencies corresponding to isotopically substituted species can be calculated very rapidly (i.e., in a few seconds on a personal computer), even for very complex substances, once the force constant matrix has been determined.

In first-principles methods, uncertainty in calculated frequencies is typically the main factor limiting the accuracy of calculated fractionation factors. As mentioned above, isotope effects on vibrational frequencies can be calculated self-consistently, using a single set of force constants for each system. The errors on the vibrational frequencies are expected to be highly systematic and largely cancel when calculating isotope frequency shifts. Méheut et al. (2009) showed that a systematic correction of n% on the frequencies induces a relative systematic correction on the logarithmic β-factors ($\ln \beta$) varying between n% (at low temperatures) to 2n% (at high temperatures). The commonly used generalized gradient approximation is for instance associated with a systematic underestimation of ~5% of the harmonic vibrational frequencies. This would lead to a relative uncertainty of ~0.5‰ on a β-factor of 10‰. Two approaches are sometimes adopted for correcting this systematic frequency error. In some studies, calculated frequencies are rescaled to experimental ones in order to improve the accuracy of the calculated fractionation factors (e.g., Schauble et al. 2006; Black et al. 2007; Blanchard et al. 2009; Li et al. 2009; Méheut et al. 2009). We must however keep in mind that calculated frequencies are harmonic, as they should be when using equations based on the harmonic approximation (e.g., Equations (5) to (10)), while experimental frequencies are influenced by anharmonicity (Liu et al. 2010). In addition, the value of the scaling parameters may be associated with significant uncertainty, depending on the quality and precision of spectroscopic data available for the compound of interest. Some studies that focus on crystals choose to correct the theoretical results by fixing the unit cell parameters to the experimental values and by optimizing only the atomic positions (e.g., Kowalski and Jahn 2011; Blanchard et al. 2015; Pinilla et al. 2015), but this procedure will usually not completely correct systematic errors in the electronic structure method, and it will of course not be applicable in materials where unit cell parameters are not known *a priori*.

Theoretical studies of non-traditional stable isotope fractionation

A big advantage to quantum-mechanical molecular modeling is the ability to derive a wide range of electronic, structural, energetic, vibrational properties from the same model. These properties can often be directly compared with observations to test the accuracy of the model. First-principles calculations also represent efficient tools to tackle crystal chemical parameters and mechanisms controlling isotopic fractionations. Over the past decade or so DFT studies have been applied to theoretical studies of stable isotope fractionation spanning most of the non-traditional stable isotopes systems represented in this volume. The results of these theoretical studies might best be discussed within the perspective of each system, considering isotopic measurements on

natural and synthetic samples as well, and this will be done in the following chapters. Here we present a brief annotated bibliography in order of increasing atomic mass, highlighting some of these works:

- Lithium: Theoretical studies focused on the equilibrium fractionation of lithium isotopes in aqueous solution (Yamaji et al. 2001) and between aqueous fluids and various Li-bearing minerals such as staurolite, spodumene and mica (Jahn and Wunder 2009; Kowalski and Jahn 2011). Isotopic results were discussed in light of the speciation change of the aqueous lithium at high temperature and pressure.

- Boron: Most of the first-principles studies investigated the equilibrium distribution of ^{10}B and ^{11}B isotopes between boric acid and borate in aqueous solution at ambient conditions, motivated by the application of boron isotope composition of marine carbonates as paleo-pH proxy (Zeebe 2005; Liu and Tossel 2005; Rustad and Bylaska 2007; Rustad et al. 2010). Tossel (2006) studied the isotopic fractionation associated with the boric acid adsorption on humic acids, and more recently Kowalski et al. (2013) investigated the B isotope fractionation between minerals, such as tourmaline and micas, and boron aqueous species at high pressure and temperature.

- Magnesium: Black et al. (2007) studied the equilibrium Mg isotope fractionation in chlorophylls. This and several later studies made efforts to improve methods to determine isotopic fractionation in liquids, with a particular focus on the fractionation between aqueous Mg^{2+} and Mg-bearing carbonate minerals (Rustad et al. 2010; Schauble 2011; Pinilla et al. 2015, Schott et al. 2016). Mg isotopes in mantle silicates were treated in Schauble (2011), Huang et al. (2013) and Wu et al. (2015).

- Silicon: Méheut et al. (2007, 2009, 2014) computed the equilibrium Si isotope fractionation factors in various silicate minerals, including phyllosilicates. Their data analysis enabled to identify the key structural and chemical parameters controlling the isotopic signatures. Huang et al. (2014) and Wu et al. (2015) applied the DFT method to silicate minerals of the Earth's mantle. Some DFT calculations coupled with isotopic measurements on meteorite and terrestrial samples focused on Si isotope fractionation between metal and silicates, in order to discuss the composition of the Earth's core and the Earth formation (e.g., Georg et al. 2007; Ziegler et al. 2010). The equilibrium fractionation in silicic acid and its potential application as proxies for paleo-pH were investigated in Dupuis et al. (2015) and Fujii et al. (2015). He and Liu (2015), He et al. (2016) complemented equilibrium Si isotope fractionation factors among minerals, organic molecules and the H_4SiO_4 solution. Javoy et al. (2012) determined the Si isotope properties of small gaseous molecules and crystalline compounds in the cosmochemical context of the solar nebula.

- Calcium: Theoretical Ca isotope fractionation factors between minerals and solution are presented in Rustad et al. (2010), in Colla et al. (2013), and among pyroxenes in Feng et al. (2014). Griffith et al. (2008) estimated fractionation factors between barite and calcite.

- Vanadium: Wu et al. (2015) explored how V isotope fractionation depends on crystal-chemical parameters such as valence, bond length and coordination number. They considered several inorganic V aqueous species and the adsorption of V^{5+} to goethite, by adopting a cluster model with explicit solvation shells.

- Chromium: Schauble et al. (2004), and Ottonello and Zuccolini (2005) computed the equilibrium Cr isotope fractionation factors of some molecules in the system Cr-H-O-Cl as well as in magnesiochromite (Ottonello et al. 2007). Moynier et al. (2011) extended

these theoretical predictions to additional Cr-bearing minerals. These latter data associated with isotopic measurements on a range of meteorites suggest that Cr depletion in the bulk silicate Earth relative to chondrites results from its partitioning into Earth's core.

- Iron: Several DFT studies focused on isotopic fractionation among Fe species in aqueous solution (Anbar et al. 2005; Domagal-Goldman and Kubicki 2008; Hill and Schauble 2008; Ottonello and Zuccolini 2008, 2009; Hill et al. 2010; Fujii et al. 2014), others looked at iron-bearing minerals such as hematite, goethite, pyrite and siderite (Blanchard et al. 2009, 2010, 2015). Rustad and Yin (2009) investigated the isotopic properties of ferropericlase and ferroperovskite in lower-mantle conditions to discuss the Earth accretion and differentiation. Fe isotope fractionation between mineral and aqueous solution was the object of the studies by Rustad and collaborators (Rustad and Dixon 2009; Rustad et al. 2010). Moynier et al. (2013) estimated the magnitude of the isotopic fractionation between different Fe species relevant to the transport and storage of Fe in higher plants. In addition to all these first-principles calculations, Mössbauer spectroscopy (e.g., Polyakov 1997, 2000) and nuclear resonant inelastic X-ray scattering, NRIXS (e.g., Polyakov et al. 2005; Dauphas et al. 2012) represent alternative techniques for obtaining Fe reduced partition function ratios.

- Copper: Seo et al. (2007) determined the equilibrium isotope fractionation of Cu^{+} complexes relevant of hydrothermal ore-forming fluids. Sherman (2013) modeled Cu-bearing minerals and various aqueous Cu^{+} and Cu^{2+} complexes to predict the equilibrium isotopic fractionation of Cu resulting from oxidation of Cu^{+} to Cu^{2+} and by complexation of dissolved Cu. Additional Cu complexes were considered in Fujii et al. (2013, 2014).

- Zinc: Several theoretical works studied the isotope fractionation of Zn between various aqueous zinc complexes including aqueous sulfide, chloride, and carbonate species relevant to hydrothermal conditions (Black et al. 2011; Fujii et al. 2010, 2011, 2014). Other complexes were modeled to discuss the Zn isotope fractionation in roots and leaves of plants (Fujii and Albarède 2012).

- Germanium: Li et al. (2009) determined equilibrium fractionation factors for a range of Ge-bearing compounds (aqueous species and minerals) simulated using cluster models. Li and Liu (2010) investigated the fractionation associated with Ge adsorption onto Fe(III)-oxyhydroxide surfaces. A cluster model was used to model the adsorption complex. Such adsorption processes occur in many environments, and thus may influence significantly the Ge isotope global budged.

- Selenium: Equilibrium Se isotope fractionation factors of inorganic and organic Se-bearing species in gaseous, aqueous and condensed phases were computed (Li and Liu 2011).

- Strontium: A combined theoretical and experimental study focused on the Sr isotope fractionation during inorganic precipitation of barite, where several strontium-bearing minerals and crystalline strontium hydrates were modeled (Widanagamage et al. 2014). This work was preceded by the determination of the isotopic fractionation between SrO_2 and a Sr^{2+} aqueous species (Fujii et al. 2008).

- Molybdenum: Mo isotope fractionation factors were determined using a cluster approach, for many aqueous species including several forms of molybdic acid and polymolybdate complexes (Tossel 2005; Weeks et al. 2007, 2008; Wasylenki et al. 2008, 2011). These results confronted with experimental data aim at identifying the molecular

mechanisms responsible to the Mo isotope fractionation during adsorption to manganese oxyhydroxides, which is a primary control on the global ocean Mo isotope budget.

- Cadmium: Yang et al. (2015) computed using DFT the equilibrium isotopic fractionation factors for Cd species relevant to hydrothermal fluids.

- Rhenium: Theoretical Re isotope fractionation has recently been investigated by Miller et al. (2015). They especially assessed the magnitude of nuclear volume fractionation with respect to mass dependent fractionation.

- Mercury and Thallium: Schauble (2007) performed first-principles calculations on these very heavy elements and could show that isotopic variation in nuclear volume is the dominant cause of equilibrium fractionation, exceeding mass-dependent fractionations. This is supported by two more recent works by Fujii et al. (2013) and Yang and Liu (2015). Wiederhold et al. (2010) performed additional theoretical calculations, quantifying the relationship between ionic bonding and equilibrium mercury isotope fractionation.

- Uranium: Abe and his collaborators (Abe et al. 2008a, 2008b, 2010, 2014) investigated the uranium isotope fractionations caused by nuclear volume effects.

Modeling isotopic properties of liquid phases

Many natural processes involve the participation of fluids. Isotopic signatures of minerals are very often related to fluid-rock interactions. Understanding the isotope fractionation processes between minerals and fluids is then of great importance. This understanding will include our ability to produce reliable theoretical mineral-solution isotopic fractionation factors. However calculations of fractionation properties of liquids and solvated elements under thermodynamic equilibrium represent a bigger challenge than for gaseous molecules or minerals. In an aqueous solution, an ion or molecule dissolved in water will interact with water molecules and other dissolved species in a continuously changing arrangement of hydrogen bonds and ion pairs. This disordered and dynamic character complicates significantly the problem. Determining the vibrational frequencies of such systems from first-principles calculations has a computation cost far greater than for minerals. Additional approximations are needed and can include the use of molecular clusters of finite size or the use of relaxed configurations from molecular dynamics simulations.

Most of the theoretical predictions of isotope fractionation in aqueous species are based on the cluster approximation (e.g., Yamaji et al. 2001; Anbar et al. 2005; Black et al. 2007, 2011; Seo et al. 2007; Domagal-Goldman and Kubicki 2008; Hill and Schauble 2008; Ottonello and Zuccolini 2009; Fujii et al. 2010, 2014, 2015; Li and Liu 2010; Rustad et al. 2010; Sherman 2013). In this case, the ion or molecular complex of interest is surrounded by water molecules forming a solvation shell and the whole is sometimes immersed in a continuum approximating the dielectric properties of the solvent. The stable structure of this isolated nanodroplet is obtained at T = 0 K by minimizing the forces acting on the atoms and the reduced partition function ratio (β-factor) is computed from the vibrational frequencies obtained in the harmonic approximation. The inclusion of the first solvation shell around the considered species is a first step towards the consideration of the solvation effect, i.e. effect explaining that most gases exhibit measurable isotopic fractionations between the vapor phase and solution. This approach

is however hindered by several difficulties, such as the number of water molecules that must be included, the symmetry of the cluster, and the consistency between different aqueous species or between the aqueous species and the mineral. Let's take the example of iron isotopes. First-principles calculations performed on small clusters give equilibrium isotopic fractionation between $Fe(H_2O)_6^{3+}$ and $Fe(H_2O)_6^{2+}$ of 2.5-3‰ at 22°C for the isotopic ratio $^{56}Fe/^{54}Fe$ (Anbar et al. 2005; Domagal-Goldman and Kubicki 2008; Hill and Schauble 2008). These values are in good agreement with the experimental value of 3.00±0.23‰ (Welch et al. 2003), even if the theoretical value depends on the cluster symmetry chosen. Here the two iron species only differ from the charge and are treated in a consistent way, which allows a cancellation of errors. However when the same theoretical data are combined with mineral β-factors (Polyakov and Mineev 2000; Polyakov et al. 2007; Blanchard et al. 2009), the calculated fractionations for Fe^{3+}-hematite and Fe^{2+}-siderite are in disagreement with experimental data. Preceded by few theoretical works emphasizing the importance of explicitly treating secondary solvation shells (e.g., Schauble et al. 2004; Liu and Tossell 2005), Rustad et al. (2010) could show that the β-factors can be reliably computed from systems as small as $M(H_2O)_6^{2+}$ but when they are embedded in a set of fixed atoms representing at least the second solvation shell (Fig. 2). Furthermore their results suggest that the aqueous cluster is much more sensitive to improvements in the basis set than the calculations on the mineral systems. By applying these results, Rustad et al. (2010) obtained more accurate β-factors for aqueous Fe^{2+} and Fe^{3+} and could reconcile theory and experiment for the mineral-solution fractionations (Fig. 2). Obviously, an observed disagreement between theory and experiment may have other reasons, such as kinetic effects during nucleation and crystal growth that could make the equilibrium assumption invalid. For example, if minerals form via oligomers or clusters as an intermediate step between the aqueous species and the mineral, then using a model of the bulk aqueous species will never reproduce the observed fractionation (e.g. Domagal-Goldman et al. 2009). More generally this cluster approach can be justified for dissolved molecules that remain more or less intact in solution (e.g., $[ClO_4]^-$, $B(OH)_3$ and CCl_4) or for aqueous complexes where intra-complex bonds are probably much stronger than interactions with bulk solvent (e.g., $[Cr(H_2O)_6]^{3+}$, $[FeCl_4]^-$, and Mg^{2+} in chlorophyll). On the other hand, this method has the disadvantage of neglecting the constant exchange of particles within the solvation shells and other effects, such as the formation of chemical bonds and structural rearrangements as a function of temperature and pressure considered to be important for the calculation of the isotope fractionation.

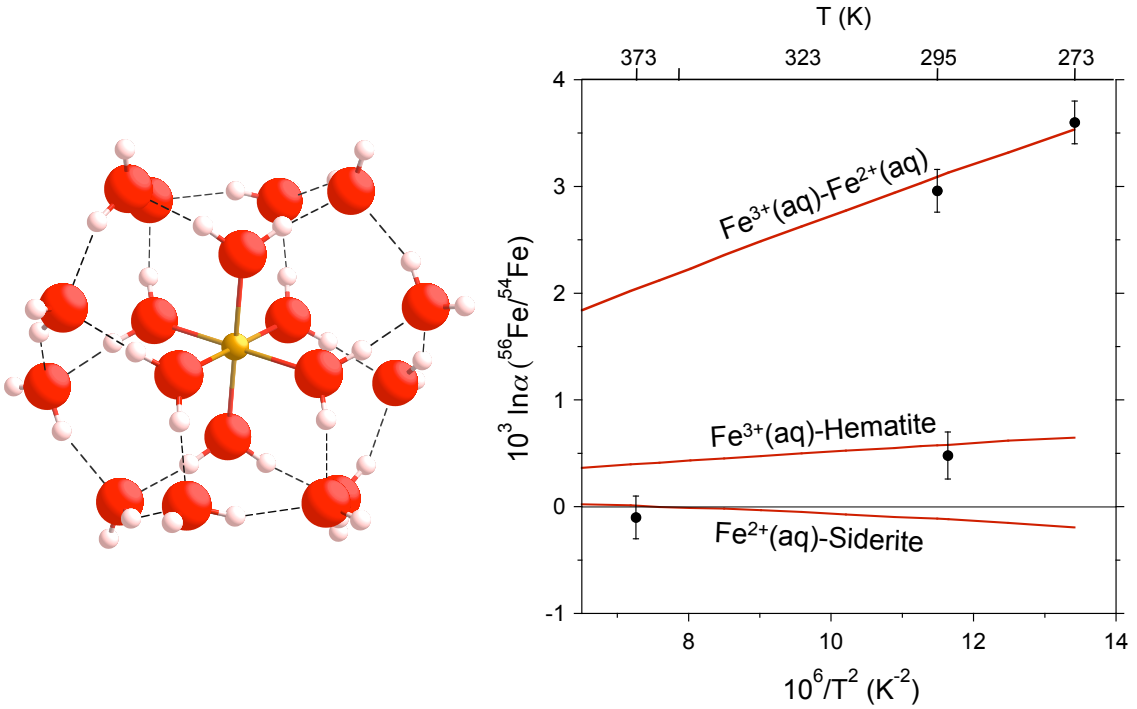

Figure 2. Left: Example of molecular cluster used by Rustad et al. (2010) to model aqueous Fe^{2+} and Fe^{3+}. Right: Calculated (curves) and measured (circles) fractionations for the pairs Fe^{3+}(aq)-Fe^{2+}(aq), Fe^{3+}(aq)-hematite and Fe^{2+}(aq)-siderite. Theoretical β-factors are from Rustad et al. (2010) for aqueous ions, from Polyakov and Mineev (2000) for siderite, and from Polyakov et al. (2007) for hematite. These two latter Mössbauer-derived β-factors are consistent with DFT results (Blanchard et al. 2009). Experimental data are from Skulan et al. (2002), Welch et al. (2003) and Wiesli et al. (2004).

To account for these dynamical phenomena, i.e. frequent particle exchange in the hydration shell and structural evolution of the fluid with pressure and temperature like it is for instance the case in Li aqueous solution (Jahn and Wunder 2009) one can go beyond the static calculations on molecular clusters by employing molecular dynamic simulations. In this case, a first-principles molecular dynamics is run at finite temperature where the condensed phase of the fluid is described through periodic boundary conditions. The equilibrated trajectory thus provides a representative distribution of the configurational environments of the species of interest in the fluid. The average fractionation factor is then estimated from the harmonic vibrational frequencies computed on a set of uncorrelated snapshots taken from the molecular dynamic trajectory. Vibrational frequencies can be computed directly from each snapshot without relaxing the atomic positions but this raises a problem because the dynamic structures are often statically unstable, meaning that some calculated frequencies are imaginary numbers. It is not clear how to make reliable thermodynamic calculations of fractionation factors when imaginary frequencies are encountered. A way around this problem is to further process each snapshot structure by allowing atomic positions to relax into the nearest local energy minimum by performing geometry optimization at T = 0 K (giving the so-called inherent structures, Stillinger and Weber 1983) before computing vibrational frequencies. This approach is more satisfactory for determining the fractionation properties from the equations based on the harmonic approximation, but on the other hand this approach erases some of the desired dynamical sampling, evident for instance in the more homogeneous bond lengths found after snapshot relaxations. An

alternative approach was proposed by Kowalski and Jahn (2011) and consists in relaxing only the position of the element of interest before determining the fractionation properties from the high-temperature approximation based on force constants. When this approximation is valid, it reduces significantly the computational cost, which is the major drawback of the molecular dynamics method. In order to keep the calculations as tractable as possible, all parameters must be chosen carefully, including the size of the simulation cell and the snapshot sampling. The simulation cell should be large enough to avoid significant interaction between atoms and their periodic images. The first studies of this kind used simulation cells containing typically 32 or 64 water molecules (Rustad and Bylaska 2007; Kowalski and Jahn 2011; Pinilla et al. 2014, 2015; Dupuis et al. 2015). However Kowalski and Jahn (2011) have shown that for a dissolved Li^+ ion a cell containing only 8 water molecules is enough to get a converged result within the accuracy of the calculations. This highlights the local character of fractionation properties, i.e. isotopic fractionation is mainly controlled by the bonds formed with the first atomic neighbors. The snapshot sampling should be large enough to get a representative distribution of the fluid configurations but small enough to keep the computation time under reasonable limits. Dupuis et al. (2015) tested thoroughly this sampling by considering a random, periodic or selected extraction of the snapshots. Results suggested that the extraction of only 10 snapshots is statistically representative of the whole solution, and that this number can even be decreased by taking advantage of the correlation between the fractionation value and the mean bond length (in cases where such correlation is evidenced).

The first study taking into account dynamical effects on isotope fractionation factors for non-traditional elements is by Rustad and Bylaska (2007). They calculated first the velocities correlation of exchanging isotopes and through its Fourier transform found the vibrational density of states to predict the boron isotope fractionation between $B(OH)_3$ and $B(OH)_4^-$ in aqueous solution. This led to a discrepancy between the calculated fractionation factor and the experimental one (Byrne et al. 2006; Klochko et al. 2006), which was solved after computing the harmonic frequencies of inherent structures taken from the molecular dynamics trajectory. Kowalski and coworkers took advantage of computing partial vibrational properties to investigate the lithium and boron isotope fractionation between aqueous fluids and minerals at high pressure and temperature (Kowalski and Jahn 2011; Kowalski et al. 2013). More recently, Pinilla et al. (2015) studied the equilibrium isotope fractionation between aqueous Mg^{2+} and carbonate minerals, and Dupuis et al. (2015) focused on silicon isotope fractionation in dissolved silicic acid. In conclusion, first-principles molecular dynamics simulations represent an efficient way to take into account the dynamical aspect of the fluid and their compressibility. By employing periodic boundary conditions, this approach also allows to treat minerals and fluids in a consistent manner; a prerequisite for reliable isotope fractionation factors between mineral and solution. All methods mentioned so far are based on the harmonic approximation. For many substances, uncertainties associated with calculated vibrational frequencies are likely to be larger than anharmonic effects. In liquids, anharmonicity effects are expected to have stronger impacts on fractionation properties. Generally anharmonicity will tend to decrease the vibrational frequencies and consequently the reduced partition function ratios (e.g., Richet et al. 1977; Méheut et al. 2007; Balan et al. 2007). To go beyond the harmonic approximation, more sophisticated techniques exist and are presented in the next section.

Beyond harmonic approximation: Path integral molecular dynamics

As already pointed out, isotopic fractionation is a quantum effect. Nuclear quantum effects (e.g., zero-point energy, quantum tunneling) whose relative contribution increases with decreasing temperature, influence significantly the properties of many systems, especially those containing lighter elements. Moreover it is also known that anharmonicity can be substantial especially for light elements and for liquid phases. A method of choice to include quantum nuclear effects without using the harmonic approximation is the method of thermodynamic integration coupled to path integral molecular dynamics (PIMD).

The reduced partition function ratio can be written using the Helmholtz free energy instead of the partition function:

$$\ln\beta_{AX} = -\frac{F(AX) - F(AX')}{\mathrm{k}T} + \left(\frac{F(AX) - F(AX')}{\mathrm{k}T}\right)_{cl} \qquad (12)$$

where $F(AX)$ and $F(AX')$ are the free energy of a single molecule of the two isotopologues AX and AX', and the subscript *cl* refers as before to quantities calculated using classical mechanics. Unfortunately, the absolute value of the free energy is not a quantity that can be directly obtained for any arbitrary system. Relating the free energy to another physical property, such as the kinetic energy, can circumvent this problem. On this line, it can be shown that the free energy of an isotopic species depends on its kinetic energy and mass (Landau and Lifshitz 1980):

$$\frac{\partial F}{\partial m} = -\frac{\langle K \rangle}{m} \qquad (13)$$

where $\langle\rangle$ represents a thermodynamic average in the canonical ensemble (i.e. thermodynamic ensemble *NVT* corresponding to a system in thermal equilibrium: the number of particles, the volume and the temperature of the system are fixed). Inserting Eq. (13) into Eq. (12) and taking into account that in the classical limit the kinetic energy of an atom is $\langle K \rangle = 3\mathrm{k}T/2$, the β-factor is then given by:

$$\ln\beta_{AX} = \frac{1}{\mathrm{k}T}\int_{m'}^{m} d\mu \frac{\langle K(\mu) \rangle}{\mu} - \frac{3}{2}\ln\left(\frac{m}{m'}\right) \qquad (14)$$

where $\langle K(\mu) \rangle$ is the average kinetic energy of the atom X of mass μ in phase AX. In this expression, the β-factor is thus obtained by thermodynamic integration from mass m' to mass m. Here, we stress that the kinetic energy used in the thermodynamic integration is that of the quantum system. It differs from the kinetic energy determined using standard molecular dynamic methods. These latter methods solve the classical equation of atomic motions in a force field, which can be defined either empirically or using *ab initio* electronic structure calculations. In the present case, the determination of the kinetic energy has to take into account the fact that, in a quantum system, the atomic trajectories are not defined. The atoms display some degree of delocalization (i.e. some uncertainty on their position); which is inversely related to their mass. Path integral methods enable the treatment of such effect by replacing the standard classical system by a larger number of replicated classical systems (Fig. 3). The replicated systems interact through harmonic springs connecting a given atom to its counterpart in adjacent replicas. Based on the exact isomorphism between a quantum particle and a classical ring polymer, the quantum

thermodynamic averages can be calculated exactly for any force field using path integral methods. PIMD methods are implemented in several codes such as the freely available program CP2K, CPMD (Marx and Hutter 2000), i-PI (Ceriotti et al. 2014) or PINY_MD (Tuckerman et al. 2000). A description of the PIMD methods and their implementations is out of the scope of this chapter but can be found elsewhere (Feynman and Hibbs 1965; Ceperley 1995; Tuckerman 2010). The drawback of PIMD methods is the computational cost that is almost prohibitive for treating at the *ab initio* level most of the systems relevant in geosciences. To address this issue, several studies report new developments that improve the efficiency of the methods concerning isotopic applications (e.g., Ceriotti and Markland 2013; Cheng and Ceriotti 2014; Marsalek et al. 2014).

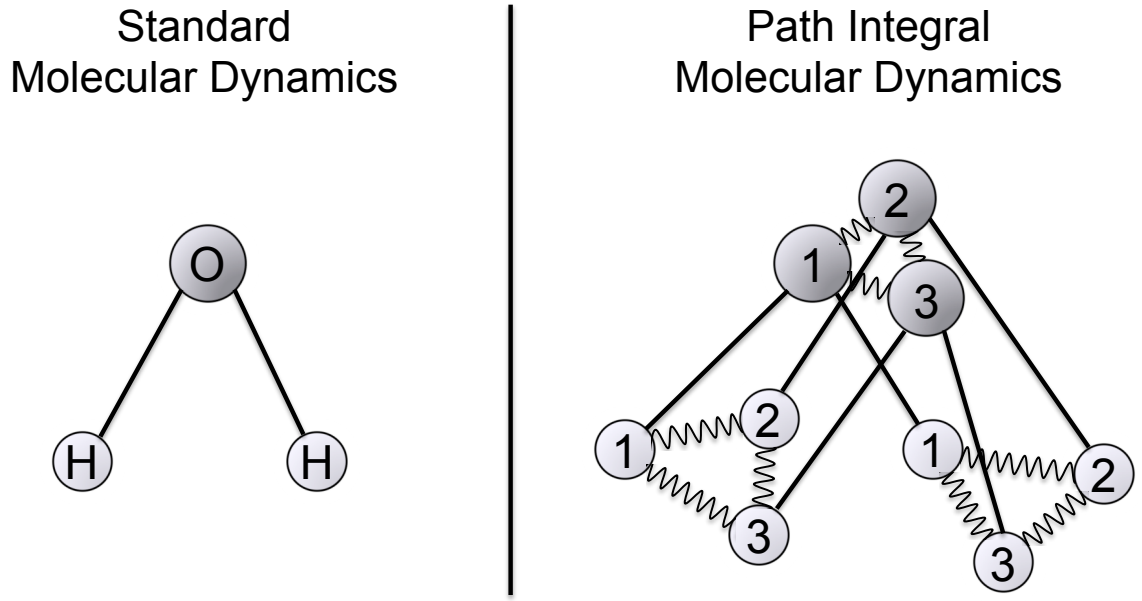

Figure 3. Schematic representations of a water molecule in standard molecular dynamics and path integral molecular dynamics. The straight lines joining the replicas (also called "beads") with the same number represent the interatomic interactions that can be modeled using either empirical or *ab initio* force fields. Replicas belonging to the same atom interact through harmonic springs. Only three replicas are represented here for clarity reasons but a large number of replicas (several tens) are actually needed to capture the quantum behavior of the system.

Regarding the investigation of isotopic effects, many studies focused on small molecules or molecular clusters, including water molecule and ions, hydrated chloride ions, carbon dioxide, organic molecules (e.g., Tachikawa and Shiga 2005; Vanicek and Miller 2007; Suzuki et al. 2008; Mielke and Truhlar 2009; Pérez and von Lilienfeld 2011; Webb et al. 2014). Other studies have modeled condensed phases, like for instance Chialvo and Horita (2009), Ramírez and Herrero (2010), Markland and Berne (2012), Zeidler et al. (2012), and Pinilla et al. (2014) for the water system. Among these studies, Pinilla et al. (2014) determined the H and O isotope equilibrium fractionation between water ice, liquid and vapor, and compared the exact result obtained from PIMD with those of the more common modeling strategies, which involve the use of the harmonic approximation. The same approach was then applied to the aqueous Mg^{2+} (Pinilla et al. 2015). Results show the importance of including configurational disorder for the estimation of isotope fractionation in liquid phases, by using molecular dynamics simulations. In the case of D/H fractionation, neglecting the anharmonic effects leads to an overestimation of the fractionation factor. In other words, the harmonic approximation will overestimate the concentration of heavy isotopes in the aqueous phase. For heavier

atoms, like magnesium and to some extent oxygen, methods based on the harmonic approximation give reliable results and in the same time reduce significantly the computational cost.

MÖSSBAUER AND NRIXS SPECTROSCOPY

In addition to the equilibrium fractionation factors derived experimentally by isotopic composition measurements, we have seen that these equilibrium constants can also be determined theoretically from the computation of the vibrational properties. An additional approach for Mössbauer-active elements (like iron, which is the most commonly studied element) consists in using Mössbauer spectroscopy (e.g., Polyakov 1997, 2000) and nuclear resonant inelastic X-ray scattering, NRIXS (e.g., Polyakov et al. 2005; Dauphas et al. 2012). These two latter techniques probe the vibrational properties of the target element and are thus ideally suited to study complex materials. Let's start again from an expression relating the reduced partition function ratio (β-factor) to the kinetic energy. Using the first-order thermodynamic perturbation theory (Landau and Lifshits 1980), Equation (14) becomes:

$$\ln\beta_{AX} = \frac{m-m'}{m}\left(\frac{K}{\mathrm{R}T}-\frac{3}{2}\right) \qquad (15)$$

In Mössbauer spectroscopy, the kinetic energy K of the active isotope (e.g. ^{57}Fe) is related to the second-order Doppler shift, $S(T)$:

$$S(T) = -\frac{K(T)}{m\mathrm{c}}$$

where c is the light velocity. Substituting $S(T)$ for $K(T)$ into Equation (15) leads to:

$$\ln\beta_{AX} = \frac{m-m'}{m}\left(\frac{m'\mathrm{c}S(T)}{\mathrm{R}T}+\frac{3}{2}\right)$$

The second-order Doppler shift S(T) can be determined experimentally from the temperature dependence of the isomer shift because both quantities only differ by a constant value that reflects the fact that the isomer shift is measured relative to a reference spectrum of metallic iron at room temperature. Experimental data are conveniently fitted using a Debye function:

$$S(T) = -\frac{9\mathrm{R}\theta_M}{16m\mathrm{c}}\left[1+8\left(\frac{T}{\theta_M}\right)^4\int_0^{\theta_M/T}\frac{x^3}{e^x-1}dx\right]$$

where m is the mass of the resonant isotope (^{57}Fe), and θ_M is a characteristic Mössbauer temperature. However, the SOD shift is not the only factor controlling the temperature shift in the Mössbauer spectra, so model assumptions about the temperature dependence of the Mössbauer isomeric shift are needed. In practice, the prediction of Mössbauer-derived fractionation factors involves an extensive data processing and requires high quality data to achieve a reasonable accuracy. This explains the few cases of conflicting results and revised data reported in the literature (e.g., Polyakov et al. 2007; Rustad et al. 2010; Blanchard et al. 2012).

In the NRIXS method, kinetic energy is calculated from the measured vibrational density of state of the element of interest using the following expression. The vibrational density of state can also be obtained by *ab initio* calculations.

$$K = \frac{3}{2}\int_0^{e_{\max}} E\left(e/\mathrm{k}T\right) g\left(e\right) de \qquad (16)$$

where $g(e)$ is the vibrational density of state of ^{57}Fe, for instance, normalized to unity, and $E(e/\mathrm{k}T)$ is the Einstein function for the vibrational energy of a single harmonic oscillator at frequency $\nu = e/\mathrm{h}$. e_{max} correspond to the maximal energy of the vibrational spectrum and the Einstein function is given by:

$$\frac{E\left(e/\mathrm{k}T\right)}{\mathrm{k}T} = \frac{e/\mathrm{k}T}{\exp(e/\mathrm{k}T)-1} + \frac{e}{2\mathrm{k}T} \qquad (17)$$

Equations (16) and (17) are valid in the harmonic approximation and Equation (16) takes into account the virial harmonic relation $K = E_{vib}/2$, where E_{vib} is the vibrational energy of the harmonic oscillator. For a given system, the β-factor calculated from the vibrational density of state (Equations 15 and 16) is identical to the β-factor calculated directly from the vibrational frequencies (Equation 10). When the highest energy of the vibrational density of state is smaller than $2\pi\mathrm{k}T$, another expression can be used, based on a Bernoulli expansion of the β-factor (Dauphas et al. 2012):

$$\ln\beta_{AX} \approx \left(\frac{m'}{m}-1\right)\left(\frac{m_2^g}{8\mathrm{k}^2T^2} - \frac{m_4^g}{480\mathrm{k}^4T^4} + \frac{m_6^g}{20160\mathrm{k}^6T^6}\right) \qquad (18)$$

where m_i^g is the ith moment of the vibrational density of state $g(e)$, given by:

$$m_i^g = \int_0^{+\infty} g(e)\ e^i\ de$$

Dauphas et al. (2012) have also shown that the even moments of $g(e)$ can be obtained directly from the moments of the NRIXS spectrum $S(e)$ and Equation (18) can be rewritten as:

$$\ln\beta_{AX} \approx \left(\frac{m'}{m}-1\right)\frac{1}{E_R}\left[\frac{R_3^S}{8\mathrm{k}^2T^2} - \frac{R_5^S - 10R_2^SR_3^S}{480\mathrm{k}^4T^4} + \frac{R_7^S + 210\left(R_2^S\right)^2R_3^S - 35R_3^SR_4^S - 21R_2^SR_5^S}{20160\mathrm{k}^6T^6}\right]$$

where E_R is the free recoil energy and R_i^S is the ith moment of $S(e)$ centered on E_R, given by:

$$R_i^S = \int_{-\infty}^{+\infty} S(e)\left(e - E_R\right)^i de$$

The NRIXS-based method probing directly the vibrational properties of the target element is expected to provide better accuracy for the β-factors than that based on Mössbauer spectroscopy. However NRIXS spectra have only recently been measured specifically for applications to isotope geochemistry (Dauphas et al. 2012). A difficulty that had been unappreciated before, was encountered concerning the baseline at low and high energies (the details of the spectrum at the low- and high-energy ends heavily influence the treatment of experimental data and therefore the value of the β-factor). To

address this issue, Dauphas and collaborators have developed a software (SciPhon) that reliably corrects for non-constant baseline (Dauphas et al. 2014; Blanchard et al. 2015; Roskosz et al. 2015).

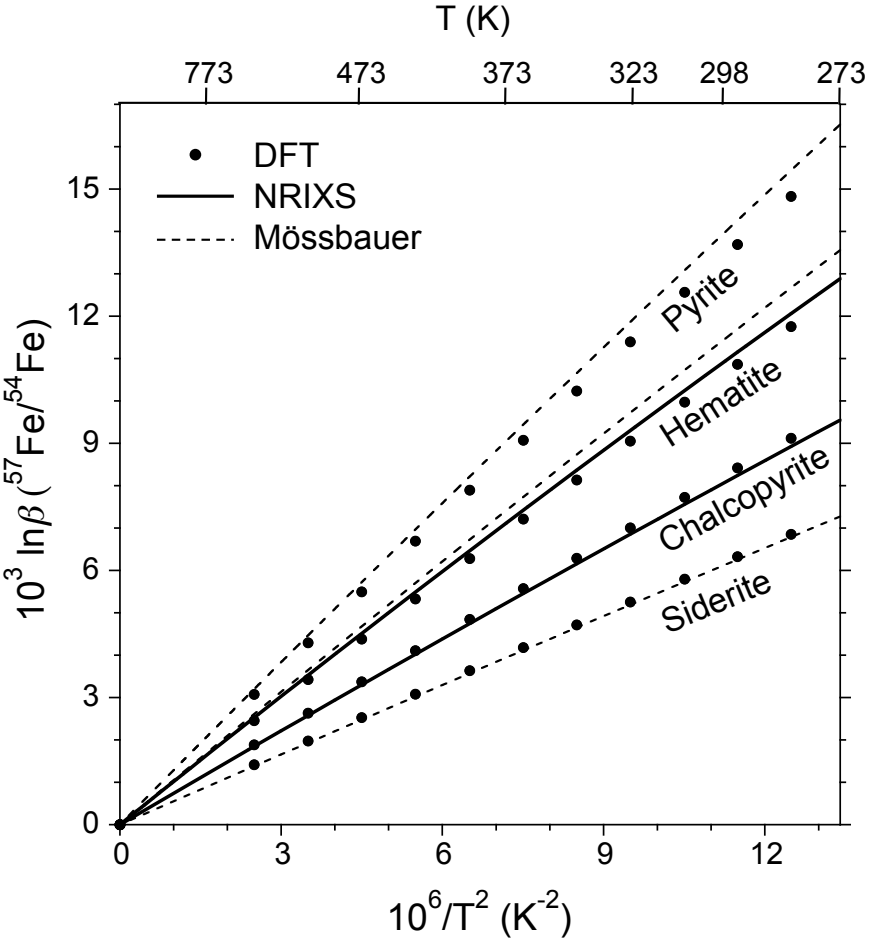

Figure 4. Comparison of iron β-factors derived from first-principles calculations (DFT), NRIXS and Mössbauer measurements for siderite ($FeCO_3$), chalcopyrite ($CuFeS_2$), hematite (Fe_2O_3) and pyrite (FeS_2). Data were taken from Blanchard et al. (2009, 2012), Dauphas et al. (2012), Polyakov and Mineev (2000), Polyakov and Soultanov (2011), Polyakov et al. (2007). In these minerals where iron atoms are always in octahedral coordination, the β-factor is mainly controlled by the iron oxidation state and the degree of covalence of the chemical bonds involved.

Figure 4 displays a comparison of the iron β-factors derived from NRIXS, Mössbauer measurements and first-principles calculations (DFT) for various iron-bearing minerals, i.e. sulfides, an oxide and a carbonate. For siderite ($FeCO_3$), DFT results (Blanchard et al. 2009) are in excellent agreement with Mössbauer data (Polyakov et al. 2007). The same kind of agreement is found between the DFT and NRIXS resuls of chalcopyrite ($CuFeS_2$, Polyakov et al. 2013). For hematite (Fe_2O_3) DFT-derived iron β-factors (Blanchard et al. 2009) are very close to NRIXS-derived values (Dauphas et al. 2012) while the results from Polyakov et al. (2007) are slightly above. In the case of pyrite (FeS_2), the apparent discrepancy between DFT and Mössbauer results that was reported in Blanchard et al. (2009) and in Polyakov and Soultanov (2011), could be resolved by using a better constrained temperature dependence of the Mössbauer spectra (Blanchard et al., 2012). The value of the iron β-factor in pyrite was confirmed by

NRIXS data (Polyakov et al. 2013) and also appears consistent with experimental measurements of equilibrium isotopic fractionation between pyrite and dissolved Fe^{2+} (Syverson et al. 2013). These comparisons exhibit that DFT, NRIXS and Mössbauer spectroscopy should lead to statistically undistinguishable β-factors, when high-quality measurements are performed followed by a careful data processing. Therefore, the comparison of results from these independent techniques provides reliable isotope fractionation factors. Figure 4 also shows that iron β-factors of these minerals are noticeably different; pyrite displaying the highest value while siderite has the lowest one. In all minerals except chalcopyrite iron atoms are in octahedral sites, the observed order can be discussed in terms of oxidation state (Fe^{3+} in hematite vs. Fe^{2+} in siderite) and degree of covalence of the interatomic bonds (low-spin, strongly covalent *d*-orbitals in pyrite vs. high-spin, ion-like *d*-orbitals in almost all other minerals).

MASS-INDEPENDENT FRACTIONATION & VARIATIONS IN MASS LAWS

Typical fractionating processes, including equilibrium isotope partitioning, activation-energy and transport-controlled disequilibrium reactions, and even gravitational and centrifugal isotope separation, almost always impart a characteristic signature in which the magnitude of isotope fractionation scales in close proportion to the difference in isotopic mass (e.g., Hulston and Thode 1965; Matsuhisa et al. 1978; Weston 1999; Young et al. 2002). A typical example is oxygen, where $^{17}O/^{16}O$ fractionation is usually 0.5-0.53 times as large as $^{18}O/^{16}O$ fractionation, very close to the ratio of mass differences (≈0.501). In high temperature igneous and metamorphic rocks the mass-fractionation relationship for oxygen is remarkably consistent, with $\delta^{17}O \approx 0.528 \pm 0.001 \times \delta^{18}O$ (e.g., Rumble et al. 2007). Subtle variations in mass dependence are observed in light stable isotope systems, including oxygen and sulfur (Barkan and Luz 2012; Hofmann et al. 2012; Farquhar et al. 2003), and are of increasing interest as potential tools to unravel the nature of fractionation in the hydrological cycle, in the precipitation of low-temperature minerals from solution, and in biochemical reactions. Young et al. (2002) pointed out that variations in mass-fractionation relationships could also help distinguish equilibrium from kinetic fractionations in non-traditional elements such as magnesium, although such measurements are likely to require very high precision in systems where fractionations of only a few per mil are observed.

Various notations have been developed to describe variations in mass dependence. Here we have followed the basic formulation of Mook (2000), which has been widely adopted. In a stable isotope fractionation involving element *X* with stable isotopes, ^{1}X, ^{2}X, and ^{3}X that have masses m_1, m_2, and m_3, there are two distinct fractionation factors α:

$$ {}^{3/1}\alpha_{AX/BX} = \frac{\left(\left[{}^{3}X\right]/\left[{}^{1}X\right]\right)_{AX}}{\left(\left[{}^{3}X\right]/\left[{}^{1}X\right]\right)_{BX}} $$

and

$$ {}^{2/1}\alpha_{AX/BX} = \frac{\left(\left[{}^{2}X\right]/\left[{}^{1}X\right]\right)_{AX}}{\left(\left[{}^{2}X\right]/\left[{}^{1}X\right]\right)_{BX}} \qquad (19) $$

In such a system it is convenient to express the mass dependence of the fractionation as a mass-fractionation exponent, θ, the ratio of the natural logarithms of the fractionation factors:

$$\theta = \frac{\ln\left({}^{2/1}\alpha_{AX/BX}\right)}{\ln\left({}^{3/1}\alpha_{AX/BX}\right)} \qquad (20)$$

Formally, mass-independent fractionation refers to any deviation of an observed fractionation from a reference mass fractionation exponent, typically expressed in delta notation:

$$\Delta'^{\,2/1} X_{AX/BX}\left(‰\right) = 10^3 \left(\theta - \theta_{reference}\right) \ln\left({}^{3/1}\alpha_{AX/BX}\right) \qquad (21)$$

Note that the prime indicates that logarithmic delta is being used here. Alternative expressions using conventional delta units may also be used, but for a discussion of fractionation factors the logarithmic delta makes the math simpler. The reference exponent might be a theoretical law or an empirically observed trend (an empirical exponent may be indicated by using λ instead of θ). There is generally not a well-accepted consensus in favor of a particular mass law exponent, so it can be tricky to compare Δ' values reported by different labs.

Variability in mass laws for common fractionations

Detailed derivations of mass law exponents for various fundamental fractionation processes have been published elsewhere (e.g., Young et al. 2002; Dauphas and Schauble 2016), and will not be reproduced here. Several of the most significant and/or common mass law exponents are listed in Table 1, below, along with calculated exponents for some traditional and non-traditional stable isotope systems. Among the most important of these is the high-temperature equilibrium mass law exponent, which can be derived from the simplified formula for isotope fractionation in Equation (11), above (Matsuhisa et al. 1978):

$$\theta_{Eq.,Hi-T} \approx \frac{\frac{1}{m_1} - \frac{1}{m_2}}{\frac{1}{m_1} - \frac{1}{m_3}} \qquad (22)$$

As noted above for Equation (11), the constant mass-dependence implied by this relationship is a surprisingly good approximation at low temperatures, even for materials with high-frequency vibrations such that $h\nu/kT > 2$ (Matsuhisa et al. 1978). In part, this occurs because the low-temperature equilibrium exponent is *identical* in the limit where the element of interest is much more massive than other atoms in the molecule (Cao and Liu 2011; Dauphas and Schauble 2016). These light-atom molecules tend to have the highest vibrational frequencies and $h\nu/kT$, especially when considering non-traditional (typically high atomic mass) isotope systems. This mass law is thus a common and sensible choice as a theory-based reference exponent (e.g., Young et al. 2002).

The mass-dependent relationships described above indicate that there will be a narrow range of variability in mass dependence for typical fractionating processes. For equilibrium fractionations of non-traditional isotopes, it is expected that the variability

will be quite small. Indeed, commonly occurring sulfur species (Z=16) show very little change in mass dependence at equilibrium at relevant temperatures (Hulston and Thode 1965; Otake et al. 2008; Farquhar et al. 2003). There has not been a focused theoretical effort to quantify the variability in elements heavier than sulfur. However, studies of oxygen and sulfur suggest that even fairly crude electronic structure models (including DFT) can give an accurate picture of mass dependence variations at equilibrium (Cao and Liu 2011), and this seems likely to be an area of future development, as measurement precision continues to improve for many non-traditional elements.

Table 1. Theoretical mass-fractionation exponents.

Type of fractionation	**θ exponent**	^{16,17,18}**O**	^{24,25,26}**Mg**	^{28,29,30}**Si**	^{32,33,34}**S**	^{54,56,57}**Fe**	^{198,200,202}**Hg**
Equilibrium, Hi-T	$\frac{\frac{1}{m_1}-\frac{1}{m_2}}{\frac{1}{m_1}-\frac{1}{m_3}}$	0.5305	0.5210	0.5178	0.5159	0.6780	0.5049
Equilibrium, Low-T, light partner	$\frac{\frac{1}{m_1}-\frac{1}{m_2}}{\frac{1}{m_1}-\frac{1}{m_3}}$	0.5305	0.5210	0.5178	0.5159	0.6780	0.5049
Equilibrium, Low-T, heavy partner †	$\frac{\sqrt{\frac{1}{m_1}}-\sqrt{\frac{1}{m_2}}}{\sqrt{\frac{1}{m_1}}-\sqrt{\frac{1}{m_3}}}$	0.5232	0.5160	0.5135	0.5121	0.6750	0.5037
Graham's law (pinhole) effusion, atomic	$\frac{\ln\left(\frac{m_1}{m_2}\right)}{\ln\left(\frac{m_1}{m_3}\right)}$	0.5158	0.5110	0.5092	0.5083	0.6720	0.5024
Graham's law effusion, high-mass molecule	$\frac{\ln\left(\frac{M_1}{M_2}\right)}{\ln\left(\frac{M_1}{M_3}\right)}$	0.5010	0.5010	0.5006	0.5007	0.6660	0.4999
Kinetic, transition state theory, jump limited	$\frac{\ln\left(\frac{\mu_1^*}{\mu_2^*}\right)}{\ln\left(\frac{\mu_1^*}{\mu_3^*}\right)}$	*Intermediate between Hi-T Eq. and high-mass molecular diffusion*					

Gravitational/centrifugal	$\frac{m_2 - m_1}{m_3 - m_1}$	0.5010	0.5010	0.5006	0.5007	0.6660	0.4999
Calculated variability		*0.0295*	*0.0200*	*0.0172*	*0.0151*	*0.0119*	*0.0050*

m_i are isotopic masses, M_i are masses of isotopically substituted molecules, and μ_i* are reduced masses of a reaction coordinate at the transition state. Based on Matsuhisa et al. (1978), Young et al. (2002), and Dauphas and Schauble (2016). † This equation only applies to the reduced partition function ratio β_{AX}, and thus to fractionation relative to atomic vapor. Actual β_{AX} exponents for non-traditional elements will rarely, if ever approach this limit because $h\nu/kT$ and/or the masses of bond partners are too small.

Mass-independent fractionation in light elements (O and S)

In addition to the subtle variations in mass dependence discussed above, there are some natural and laboratory environments that give rise to fractionations that deviate strongly from a proportional relationship with mass differences. These are called mass-independent fractionations, even though they are usually driven, ultimately, by differences in isotopic mass. The best-known examples of mass-independent fractionation are in oxygen and sulfur isotopes, and are thought to be associated with reactions between molecules in the gas phase. Large, approximately 1:1 variation in $^{17}O/^{16}O$ vs. $^{18}O/^{16}O$ is observed in primitive meteoritic oxides and silicates (Clayton et al. 1973). Although the cause of this fractionation is not yet settled, the most common explanation is that it represents a self-shielding effect in carbon monoxide, in which the common isotopologue $^{12}C^{16}O$ is optically thick to incoming light with the right energy to break it apart, while $^{12}C^{17}O$ and $^{12}C^{18}O$ are optically thin, and thus more prone to react in the interior of the solar nebula or a molecular cloud (Clayton 2002; Lyons and Young 2005). In the stratosphere, a large, ~1:1 fractionation of $^{17}O/^{16}O$ and $^{18}O/^{16}O$ is found in ozone, and in gases that exchange oxygen with ozone. It is thought that this fractionation reflects an isotopic effect on the lifetime of excited ozone molecules (Heidenreich and Thiemens 1986; Mauersberger 1987; Gao and Marcus 2001). Mass-independent sulfur isotope fractionation has been found widely in Archean and earliest Proterozoic samples (Farquhar et al. 2000). These samples show a range of $^{33}S/^{32}S$ vs. $^{34}S/^{32}S$ relationships, thought to be caused by photochemical reactions of SO_2 in the early atmosphere, before O_2 became a major constituent of air (Pavlov and Kasting 2002; Lyons 2007).

Mass-independent fractionation in non-traditional elements (Hg, Tl, and U)

For non-traditional stable-isotope systems, at least two different fractionation mechanisms seem to be responsible for mass-independent fractionation effects. Most dramatic are large (> 1‰) mass-independent mercury isotope fractionations that are mainly photochemical (e.g., Bergquist and Blum 2007), and appear to be magnetic isotope effects dependent on the non-zero spins of the odd numbered mercury isotopes ^{199}Hg and ^{201}Hg. Introductory reviews of the magnetic isotope effect have been presented elsewhere (Turro 1983; Buchachenko 1995, 2013). The effect is apparent only in a subset of disequilibrium reactions. As yet, there are not any quantitative theoretical models that can reproduce the observed mass-independent signatures, and this is an area where more work is clearly needed.

Another type of fractionation is observed in the uranium and thallium isotope systems (Stirling et al. 2007; Rehkämper et al. 2002). Variation in isotope abundances in these elements in nature appears to mainly result from an equilibrium mass-independent phenomenon: the nuclear field shift effect. This effect also acts to fractionate mercury isotopes (e.g., Estrade et al. 2009; Wiederhold et al. 2010; Ghosh et al. 2013; Schauble 2007), but the mass-independent signature is much more subtle than the largest MIFs observed in natural samples, e.g, Blum et al. (2014). This effect has been the subject of a number of first-principles theoretical studies.

Bigeleisen (1996) and Nomura et al. (1996) proposed that equilibrium isotopic fractionation in elements with very high atomic numbers could be driven by differences in the shape and size of nuclei, in addition to differences in mass. Hints of this effect were also described in an earlier experimental study of strontium isotope fractionation

(Nishizawa et al. 1995). This is the nuclear field shift effect, and it is caused by overlap of electron density with the spatial volume occupied by the positive charge of a nucleus (Fig. 5). The general effect is to reduce the binding energy of electrons around large nuclei. This nuclear volume effect appears to be the most important component of the field shift, but non-spherical shapes may also be important for field shift effects in some nuclei; this shape-dependent part of the field shift is not as well studied as the volume component (e.g., Knyazev et al. 1999). Bigeleisen, Nomura, and their collaborators used the field shift effect to explain laboratory uranium isotope fractionation experiments in which the oxidized form of uranium, U(VI), had lower $^{238}U/^{235}U$ than coexisting reduced species at equilibrium. Such inverted redox/fractionation relationships are rare. A key observation was that $^{236}U/^{238}U$, $^{238}U/^{234}U$, $^{238}U/^{235}U$, and $^{238}U/^{233}U$ fractionations did not obey a consistent mass dependent relationship, with the magnitude of $^{238}U/^{235}U$ fractionation for instance being very similar to $^{238}U/^{234}U$, despite a 3:4 mass difference ratio (Nomura et al. 1996).

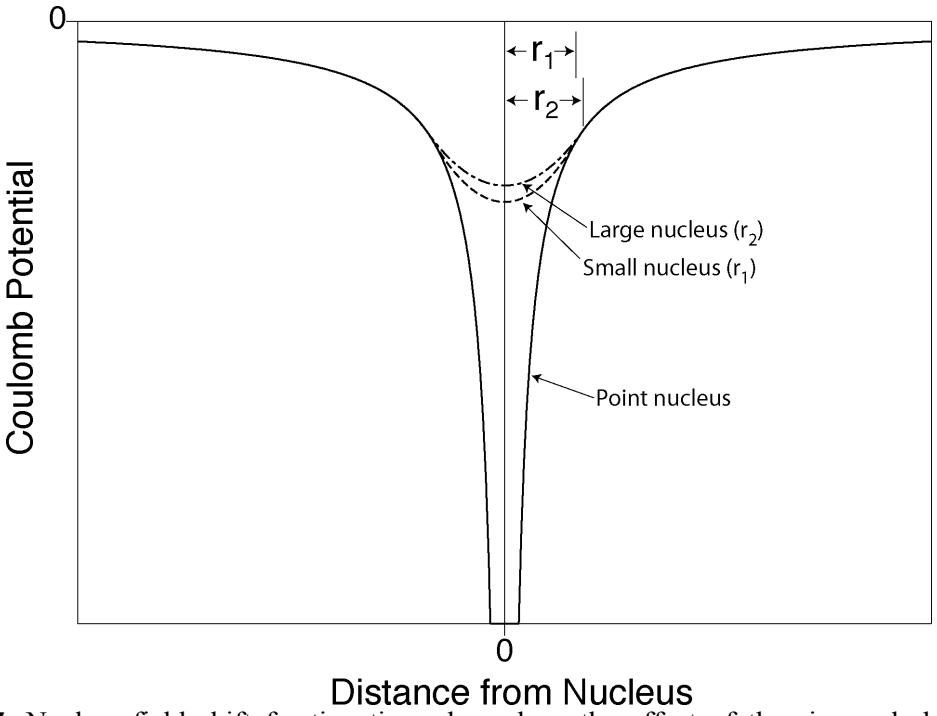

Figure 5. Nuclear field shift fractionations depend on the effect of the size and shape of a nucleus on the binding energy of electrons. The simplified example shown here assumes a single electron attracted to a spherical nucleus with a uniform charge density. The solid line shows the electrostatic potential binding an electron to an infinitesimally small nucleus, which goes to negative infinity as the electron approaches the nuclear center. For finite nuclei, the Coulomb potential does not go to negative infinity, but instead approaches a finite minimum inside the nucleus because the net electrostatic attraction to the shell of nuclear charge farther from the center than the electron is zero. The minimum is higher (the binding potential is weaker) for a large nucleus than for a small nucleus. Here the radius difference is assumed to be 10%, which is much larger than the difference between stable isotopes of most elements. Adapted from Schauble (2007).

Isotope fractionations caused by the field shift effect can be quantified if field shift energies are known:

$$\ln\alpha_{FS} = \frac{\left[E^0(AX) - E^0\left(AX^*\right)\right] - \left[E^0(BX) - E^0\left(BX^*\right)\right]}{\mathrm{k}T} \qquad (23)$$

where α_{FS} is the field shift fractionation factor, and $E^0(AX)$, etc. are the ground state electronic energies of isotopic forms of *AX* and *BX*. Approximate expressions for the field shift energies have been derived in the optical spectroscopy literature (e.g., King 1984); these formulations capture the dependence of the field shift effect on the size of the nucleus (i.e., spatial nuclear volume) and on the electron density that overlaps it, e.g.,

$$\ln\alpha_{FS} \approx \frac{2\pi Ze^2}{3\mathrm{k}T}\left(\left|\Psi(0)_{AX}\right|^2 - \left|\Psi(0)_{BX}\right|^2\right)\Delta\left\langle r^2\right\rangle \qquad (24)$$

where Z is the nuclear charge, e is the charge of an electron, $|\Psi(0)_{AX}|^2$ and $|\Psi(0)_{BX}|^2$ are the electron densities at the center of the nucleus of the atom of interest in substances *AX* and *BX*, and $\Delta\langle r^2\rangle$ is the difference in mean-squared nuclear charge radius between the fractionating isotopes. This expression is approximate because it assumes a simplified model of the distribution of charge density in nuclei, that the nuclei are spherical (nuclei with odd numbers of neutrons and/or protons are aspherical) and that the electronic structure does not change as the nuclear size changes. The assumption of sphericity means that only the nuclear volume component of the field shift is considered, and potential shape effects are ignored.

Given these assumptions, however, it is clear that large nuclear field shift fractionations are most likely to occur between substances where the electron densities at the nucleus are very different, and where the difference in nuclear charge radius is large. Because the wavefunctions *d*- and *f*-orbital electrons (and most *p*-orbital electrons) do not overlap significantly with nuclei, variations in *s*-orbital electron population and structure control field shift fractionations. Based on Equation 24, and theoretical studies made so far, it is possible to list some qualitative rules of thumb about the chemical and physical properties that control field shift isotope fractionations:

1) Field shift isotope effects scale with nuclear charge radius, not with isotopic mass. Nuclear charge radii usually (but not always) increase with increasing neutron number, but tend to be smaller for nuclei with odd numbers of neutrons than one would expect from the radii of neighboring even-neutron number nuclei. For this reason, field shift fractionations will often generate a characteristic odd-even fractionation pattern (e.g., Nomura et al. 1996; Bigeleisen 1996). Not all elements show this pattern, however. For platinum, radii are almost perfectly linear for both odd and even numbered nuclei. In contrast, the ^{52}Cr nucleus, with a "magic" number of 28 neutrons, is notably smaller than stable chromium isotopes with fewer or greater numbers of neutrons.

2) Changes in *s*-electron occupation and *s*-orbital shapes control field shift fractionation.

3) Species with more *s*-electrons, and more compact s-orbitals, will tend to attract smaller nuclei. Examples include Hg(0) vs. Hg (II) and Tl(I) vs. Tl(III) -- in each case the reduced form has two 6*s* electrons while the oxidized form has none, so Hg(0) and Tl(I) species preferentially incorporate small (neutron poor) isotopes. This pattern is likely for the 0 to +2 oxidation states of most elements in groups 1-12 of the periodic table, for the +1 to +3 oxidation states of group 13 elements, and for the +2 to +4 oxidation states of the group 14 elements. Field shift fractionation and mass-dependent fractionation will

often tend to reinforce each other for elements and species in this category, leading to larger observed fractionations. *p*-, *d*-, and *f*-electronic orbitals affect field shifts indirectly; more electrons in these orbitals, and more compact orbital structures, tend to push *s*-electrons away from the nucleus. So species with more *p*-, *d*-, and/or *f*-electrons will tend to attract larger nuclei. U(IV) vs. U(VI) is an example of this behavior, with the two valence 5*f*-electrons in U(IV) species leading to higher $^{238}U/^{235}U$ than in 5*f*-depleted U(VI) species. This pattern is likely to occur in oxidation states higher than +2 for elements in groups 3-11, lanthanides, and actinides, as well as for the –4 to +2 oxidation states of group 14 elements, the –3 to +3 oxidation states of group 15 elements, the –2 to +4 oxidation sates of group 16 elements, and the –1 to +5 oxidation states of group 17 elements. In these systems, field shift effects and mass-dependent fractionation may tend to oppose each other and partially cancel.

4) Valence *s*-orbital electron densities vary much more widely in heavy (high-Z) elements than light (low-Z) elements. So field shift isotope fractionation effects will be much larger for elements with high atomic numbers (Knyazev and Myasoedov 2001; Schauble 2007). Isotopic variation in nuclear charge radii also varies a lot from one isotope pair to another, but it does not show a strong general trend with atomic number (Knyazev and Myasoedov 2001). It is not yet clear what the minimum atomic number needs to be for significant field shift effects to occur.

5) Field shift fractionation factors scale with T^{-1}, whereas equilibrium mass-dependent fractionations tend to scale as T^{-2} (Eq. 11). As temperature increases, field shift effects may overwhelm mass-dependent fractionation for some elements.

Mass-independent fractionation signatures in heavy elements, versus light elements

In light elements (e.g., oxygen and sulfur), mass-independent fractionations (despite the terminology) ultimately follow from effects of mass differences on reaction rates and photochemical cross sections. In contrast, mass-independent fractionation effects in elements with high atomic numbers appear to be determined mainly by nuclear properties other than mass, including nuclear spin, volume, and shape. This can lead to some confusion, because mass-independent phenomena in heavy elements may or may not lead to observable departures from proportionality to isotopic mass differences. Illustrative examples can be found in the thallium and mercury isotope systems. Thallium isotope fractionation in nature is likely dominated by the field shift effect (Rehkämper et al. 2002; Schauble 2007; Nielsen et al. 2015), but there are only two stable thallium isotopes, ^{203}Tl and ^{205}Tl, making observation of mass-disproportionate fractionation impossible in natural samples and impractical in laboratory experiments. Among the four common even-numbered isotopes of mercury (^{198}Hg, ^{200}Hg, ^{202}Hg, and ^{204}Hg), isotope fractionations caused by field shift, magnetic, and mass-dependent isotope effects cannot be distinguished solely on the basis of apparent mass-fractionation relationships, because nuclear volume increases by an almost constant increment with each additional pair of neutrons and the magnetic isotope effect is limited to the odd-numbered isotopes ^{199}Hg and ^{201}Hg.

***Ab initio* methods for calculating field shift fractionation factors**

Bigeleisen (1996) and Nomura et al. (1996) identified the nuclear field shift effect in uranium isotope fractionations based on the inverse relationship between $^{238}U/^{235}U$ and oxidation state, and the close correlation between the magnitude of fractionation in other uranium isotopes and nuclear charge radii variations inferred from optical spectra of uranium vapor. Because of the characteristic pattern of isotopic charge radii, which deviates from pattern of mass differences, they were able to draw conclusions without a quantitative, *ab initio* theoretical model of the species present in the experiments. Such charge radius pattern matching has been widely used to search for evidence of field shift isotope fractionations in laboratory experiments and natural samples (Fujii et al. 2009; Fujii et al. 2006a,b), and it has been useful for ruling out the field shift effect as the main cause of mass-independent signatures in mercury (e.g., Blum et al. 2014). However, it is not well suited to predict how large field shift effects will be in previously unstudied reactions and isotope systems. The ability to make forward models is important in these situations, and may also be necessary in systems where processes that mimic field shift fractionation patterns might be active, such as during nucleosynthesis. Reasonably accurate compilations of nuclear charge radii for almost all stable and long-lived radioactive nuclei are available in the literature (Fricke and Heilig 2004; Angeli and Marinova 2013.; Nadjakov et al. 1994 and updates), so the main goal of theoretical models is to determine electron densities in the species of interest.

Accurate calculations of electron densities bound to high atomic number nuclei must take account of relativity effects. This can be understood by noting that the kinetic energy of a loosely bound *s*-orbital electron, when it is momentarily near the center of a highly charged nucleus, will be of the same order of magnitude as its rest mass energy. Even the *average* kinetic energies of inner-shell *1s*-orbital electrons are ~100 keV (vs. 511 keV rest mass energy) in elements such as Hg, Tl and U. That implies a velocity that is a significant fraction of the speed of light. For this reason, most *ab initio* studies of field shift effects to date have been based on the Dirac equation, a relativistic counterpart to the more familiar Schrödinger equation.

Some early theoretical studies of field shift fractionation are based on atomic and ionic models of electronic structure (Knyazev and Myasoedov 2001; Abe et al. 2008a). These calculations are easily performed on modern personal computers, but they assume a purely ionic bonding environment. More recently, Dirac-Fock and related model chemistries have been used to directly model molecules (e.g., Schauble 2007; Abe et al. 2008b, 2010; Wiederhold et al. 2010; Fujii et al. 2010). Comparisons to atomic spectra and laboratory measurements indicate that such models are usefully accurate (Schauble 2007; Wiederhold et al. 2010). The basic procedure for constructing a relativistic electronic structure model for calculating field shift fractionation is similar to the initial steps in creating a vibrational model for predicting mass-dependent fractionation, which was outlined in the preceding sections: first an initial structure is selected, and an electronic structure calculation is used to estimate the static energy of the structure; this is often followed up by performing a structural optimization. Vibrational frequencies need not be calculated -- if mass-dependent fractionation factors are desired it is usually easier to construct a separate model based on non-relativistic theory, such as conventional DFT. The energy associated with isotope substitution can either be determined using an expression like Equation (24), or (even better) directly by manipulating the size of the nucleus in the first-principles model. Much like Hartree-Fock theory, Dirac-Fock theory has been extended to improve model accuracy by considering electron correlation effects and excited electronic states (see Wiederhold et

al. 2010 and Nemoto et al. 2015 for comparisons of model results at various levels of theory). These high-accuracy calculations are much more demanding of computation time and memory, however.

Although theoretical studies based on *ab initio* relativistic electronic structure models have shown good agreement with measurements, the calculations are notably more complex, memory-intensive, and slow than typical non-relativistic methods. As a result, only fairly small molecules (no more than ~20 non-hydrogen atoms) can be modeled easily. Solid and liquid phases must be approximated using small clusters, which is likely to increase model uncertainties. It is difficult to confidently formulate a model of substances with long-range bonding interactions, such as metals or strongly solvated aqueous species, within these constraints. Several different ways around this limitation have been proposed. The first takes advantage of strong correlations between field shift effects in mercury compounds and the effective ionic charges of mercury atoms in those structures. This makes it possible to interpolate fractionations involving complex materials, such as liquid mercury, based on effective ionic charges computed with simpler electronic structure models (Wiederhold et al. 2010; Ghosh et al. 2013). This method may be best suited for group 1, 2 and 12 elements, where the field shift effect is dominated by a single valence *s* orbital. The second method, introduced by Nemoto et al. (2015), involves the use of a simplified relativistic modeling approach (the Douglas-Kroll-Hess method) that accurately reproduces variations in electron density near high atomic number nuclei with an order of magnitude less computational effort. This raises the possibility of directly modeling larger, more complex molecules while retaining enough accuracy to be useful. The third method, proposed by Schauble (2013) uses fully relativistic Dirac-Fock models (including some electron correlation effects) of simple molecules to calibrate a corresponding set of DFT models that are built using Projector Augmented Wave (PAW) data sets (Blöchl 1994). PAW is closely related to the pseudopotential methods described earlier in this chapter, and is also typically used in conjunction with plane-wave basis sets and periodic boundary conditions. Roughly the same computational effort is required for PAW methods as for standard pseudopotential-based DFT. But PAW has the advantage that information about the structure of core electronic orbitals is preserved, so that it is possible to calculate the influence of different chemical bonding environments on electron densities at the nucleus with reasonable accuracy (e.g., Zwanziger 2009). Both PAW and pseudopotential basis sets can be constructed using a partial correction for relativistic effects near the nucleus. Like the simplified relativistic approach proposed by Nemoto et al. (2015), the calibrated PAW method can be applied to larger, more complex materials and molecules, and it can even be applied to metals (such as metallic mercury) and semi-conducting materials where long-range bonding interactions are important. However, the PAW method probably loses some accuracy due to its dependence on a limited calibration set of small molecules.

Isomer shifts from Mössbauer spectroscopy

A final method of calculating nuclear field shift fractionations, suggested originally by Knyazev and Myasoedov (2001), uses isomer shifts measured with Mössbauer spectroscopy to determine changes in electron density from one species to another. Isomer shifts and field shifts arise from the same interaction between nuclear charge and electron density, with the main difference being that in Mössbauer

spectroscopy the nuclear charge radius changes spontaneously as the Mössbauer nucleus is excited and then decays. In terms of data processing, the isomer shift is distinct from the second-order Doppler shift and NRIXS vibrational spectroscopy -- it is typically one of the fundamental parameters measured in a standard Mössbauer experiment (along with quadrupole and magnetic splitting), and does not require measurements at multiple temperatures or a synchotron X-ray source. Like second-order Doppler shift and NRIXS measurements, isomer shifts can be measured in complex materials, selectively and directly probing the Mössbauer isotope's chemical environment. Knyazev and Myasoedov (2001) showed a promising correlation between calculated electron density variations in vapor-phase neptunium ions with varying charge and measured ^{237}Np-isomer shifts in crystals where Np has the same formal oxidation states. Schauble (2013) went a step farther by comparing ^{119}Sn-isomer shifts with electron densities calculated in the same substances using the DFT-PAW approach. The excellent correlation suggests that Mössbauer spectroscopy will be a powerful tool to predict field shift isotope fractionation in elements with Mössbauer-active isotopes.

CONCLUSIONS

While the theory of stable isotope fractionation has been developed in the middle of the twentieth century, the last decade was marked by the growing use of first-principles calculations to apply the theory to non-traditional stable isotopes. The aim of these calculations was first to determine the isotope fractionation factors when the considered phases are in thermodynamic equilibrium in order to identify the factors controlling these equilibrium fractionations. Quantitatively, the theoretical studies mentioned in this chapter but also the others dealing with the traditional stable isotopes show that calculated fractionation factors are reliable enough to be directly compared to experimental values and to values derived from spectroscopic techniques such as Mössbauer and NRIXS. To reach such level of accuracy, high-quality calculations are necessary (the quality of the model can be tested by comparing the calculated structural, electronic and vibrational properties with available experimental data) and most importantly the considered phases must be treated in a consistent manner. In stable isotope geochemistry, first-principles molecular modeling now represents numerical experiments that fully complement laboratory experiments for contributing to the interpretation of isotopic data collected on natural samples.

The advances in computation power enable to model systems of increasing complexity. Among the future directions of research that deserve special efforts, we can cite the investigation of isotopic fractionations associated with complex crystal chemical processes (e.g., solid solutions, chemical impurities, crystal defects, adsorption complexes), and the exploration of the mechanisms producing mass-independent fractionation, not to mention kinetic fractionation.

ACKNOWLEDGEMENTS

This chapter was improved by the thoughtful suggestions from T. Fujii, J. Kubicki and J. Wiederhold.

REFERENCES

Abe M, Suzuki T, Fujii Y, Hada M (2008a) An ab initio study based on a finite nucleus model for isotope fractionation in the U(III)-U(IV) exchange reaction system. J Chem Phys 128:144309

Abe M, Suzuki T, Fujii Y, Hada M, Hirao K (2008b) An ab initio molecular orbital study of the nuclear volume effects in uranium isotope fractionations. J Chem Phys 129:164309

Abe M, Suzuki T, Fujii Y, Hada M, Hirao K (2010) Ligand effect on uranium isotope fractionations caused by nuclear volume effects: An ab initio relativistic molecular orbital study. J Chem Phys 133:044309

Abe M, Hada M, Suzuki T, Fujii Y, Hirao K (2014) Theoretical Study of Isotope Enrichment Caused by Nuclear Volume Effect. J Comp Chem, Japan 13:92-104

Anbar AD, Jarzecki AA, Spiro TG (2005) Theoretical investigation of iron isotope fractionation between $Fe(H_2O)_6^{3+}$ and $Fe(H_2O)_6^{2+}$: implications for iron stable isotope geochemistry. Geochim Cosmochim Acta 69:825–837

Angeli I, Marinova KP (2013) Table of experimental nuclear ground state charge radii: An update. Atom Data Nucl Data Tables 99:69-95

Anisimov VI, Zaanen J, Andersen OK (1991) Band theory and Mott insulators: Hubbard *U* instead of Stoner *I*. Phys Rev B 44:943

Balan E, Lazzeri M, Delattre S, Meheut M, Refson K, Winkler B (2007) Anharmonicity of inner-OH stretching modes in hydrous phyllosilicates: Assessment from first-principles frozen-phonon calculations. Phys Chem Minerals 34:621-625

Balan E, Blanchard M, Pinilla C, Lazzeri M (2014) First-principles modeling of sulfate incorporation and $^{34}S/^{32}S$ isotopic fractionation in different calcium carbonates. Chem Geol 374-375:84-91

Barkan E, Luz B (2012) High precision measurements of $^{17}O/^{16}O$ and $^{18}O/^{16}O$ ratios in CO_2. Rapid Commun Mass Spectrom 26:2733-2738

Baroni S, de Gironcoli S, Dal Corso A, Giannozzi P (2001) Phonons and related crystal properties from density-functional perturbation theory. Rev Mod Phys 73:515-561

Bergquist BA, Blum JD (2007) Mass-dependent and -independent fractionation of Hg isotopes by photoreduction in aquatic systems. Science 318:417-420

Bigeleisen J (1996) Nuclear size and shape effects in chemical reactions. Isotope chemistry of the heavy elements. J Am Chem Soc 118:3676-3680

Bigeleisen J, Mayer MG (1947) Calculation of equilibrium constants for isotopic exchange reactions. J Chem Phys 15:261-267

Black JR, Yin Q-Z, Rustad JR, Casey WH (2007) Magnesium isotopic equilibrium in chlorophylls. J Am Chem Soc 129:8690-8691

Black JR, Kavner A, Schauble EA (2011) Calculation of equilibrium stable isotope partition function ratios for aqueous zinc complexes and metallic zinc. Geochim Cosmochim Acta 75:769-783

Blanchard M, Poitrasson F, Méheut M, Lazzeri M, Mauri F, Balan E (2009) Iron isotope fractionation between pyrite (FeS_2), hematite (Fe_2O_3) and siderite ($FeCO_3$): A first-principles density functional theory study. Geochim Cosmochim Acta 73:6565-6578

Blanchard M, Morin G, Lazzeri M, Balan E (2010) First-principles study of the structural and isotopic properties of Al- and OH-bearing hematite. Geochim Cosmochim Acta 74:3948-3962

Blanchard M, Poitrasson F, Méheut M, Lazzeri M, Mauri F, Balan E (2012) Comment on "New data on equilibrium iron isotope fractionation among sulfides: Constraints on mechanisms of sulfide formation in hydrothermal and igneous systems" by VB Polyakov and DM Soultanov. Geochim Cosmochim Acta 86:182-195

Blanchard M, Dauphas N, Hu MY, Roskosz M, Alp EE, Golden DC, Sio CK, Tissot FLH, Zhao J, Gao L, Morris RV, Fornace M, Floris A, Lazzeri M, Balan E (2015) Reduced partition function ratios of iron and oxygen in goethite. Geochim Cosmochim Acta 151:19-33

Blöchl PE (1994) Projector augmented-wave method. Phys Rev B 50:17953-17979
Blum JD, Sherman LS, Johnson MW (2014) Mercury isotopes in earth and environmental sciences. Ann Rev Earth Planet Sci 42:249-269
Buchachenko AL (1995) Magnetic isotope effect. Theor Exp Chem 31:118-126
Buchachenko AL (2013) Mass-independent isotope effects. J Phys Chem B 117:2231-2238
Byrne RH, Yao W, Klochko K, Kaufman AJ, Tossell JA (2006) Experimental evaluation of the isotopic exchange equilibrium $^{10}B(OH)_3+^{11}B(OH)_4^-=^{11}B(OH)_3+^{10}B(OH)_4^-$ in aqueous solution. Deep Sea Res 1:684-688
Cao X, Liu Y (2011) Equilibrium mass-dependent fractionation relationships for triple oxygen isotopes. Geochim Cosmochim Acta 75:7435-7445
Ceperley D (1995) Path integrals in the theory of condensed helium. Rev Mod Phys 67:279-355
Ceriotti M, Markland TE (2013) Efficient methods and practical guidelines for simulating isotope effects. J Chem Phys 138:014112
Ceriotti M, More J, Manolopoulos DE (2014) i-PI: A Python interface for ab initio path integral molecular dynamics simulations. Comput Phys Commun 185:1019–1026
Cheng B, Ceriotti M (2014) Direct path integral estimators for isotope fractionation ratios. J Chem Phys 141:244112
Chialvo A, Horita J (2009) Liquid-vapour equilibrium fractionation of water: how well can classical water models predict it? J Chem Phys 130:094509
Clark SJ, Segall MD, Pickard CJ, Hasnip PJ, Probert MJ, Refson K, Payne MC (2005) First principles methods using CASTEP. Zeitschrift fuer Kristallographie 220:567-570
Clayton RN, Grossman L, Mayeda TK (1973) A Component of Primitive Nuclear Composition in Carbonaceous Meteorites. Science 182:485-488
Clayton RN (2002) Solar System: self-shielding in the solar nebula. Nature 415:860-861
Cococcioni M, de Gironcoli S (2005) Linear response approach to the calculation of the effective interaction parameters in the LDA+*U* method. Phys Rev B 71:035105
Colla CA, Wimpenny J, Yin Q-Z, Rustad JR, Casey WH (2013) Calcium-isotope fractionation between solution and solids with six, seven or eight oxygens bound to Ca(II). Geochim Cosmochim Acta 121:363-373
Cygan RT, Kubicki JD (2001) Molecular modeling theory: Applications in the geosciences. Rev Mineral Geochem 42
Dauphas N, Roskosz M, Alp EE, Golden DC, Sio CK, Tissot FLH, Hu MY, Zhao J, Gao L, Morris RV (2012) A general moment NRIXS approach to the determination of equilibrium Fe isotopic fractionation factors: Application to goethite and jarosite. Geochim Cosmochim Acta 94:254-275
Dauphas N, Roskosz M, Alp EE, Neuville D, Hu M, Sio CK, Tissot FLH, Zhao J, Tissandier L, Medard E, Cordier C (2014) Magma redox and structural controls on iron isotope variations in Earth's mantle and crust. Earth Planet Sci Lett 398:127-140
Dauphas N, Schauble EA (2016, in press) Mass fractionation laws, mass independent effects, and isotopic anomalies. Ann Rev Earth Planet Sci
Domagal-Goldman SD, Kubicki JD (2008) Density functional theory predictions of equilibrium isotope fractionation of iron due to redox changes and organic complexation. Geochim Cosmochim Acta 72:5201–5216
Domagal-Goldman SD, Paul KW, Sparks DL, Kubicki JD (2009) Quantum chemical study of the Fe(III)-desferrioxamine B siderophore complex—Electronic structure, vibrational frequencies, and equilibrium Fe-isotope fractionation. Geochim Cosmochim Acta 73:1-12
Dovesi R, Orlando R, Erba A, Zicovich-Wilson CM, Civalleri B, Casassa S, Maschio L, Ferrabone M, De La Pierre M, D'Arco P, Noel Y, Causa M, Rerat M, Kirtman B (2014) CRYSTAL14: A Program for the Ab Initio Investigation of Crystalline Solids. Int J Quantum Chem 114:1287-1317
Dupuis R, Benoit M, Nardin E, Méheut M (2015) Fractionation of silicon isotopes in liquids: The importance of configurational disorder. Chem Geol 396:239-254
Estrade N, Carignan J, Sonke JE, Donard OFX (2009) Mercury isotope fractionation during

liquid-vapor evaporation experiments. Geochim Cosmochim Acta 73:2693–2711
Farquhar J, Bao H, Thiemens M (2000) Atmospheric Influence of Earth's Earliest Sulfur Cycle. Science 289:756-758
Farquhar J, Johnston DT, Wing BA, Habicht KS, Canfield DE, Airieau S, Thiemens MH (2003) Multiple sulphur isotopic interpretations of biosynthetic pathways: implications for biological signatures in the sulphur isotope record. Geobiology 1:27-36
Feng C, Qin T, Huang S, Wu Z, Huang F (2014) First-principles investigations of equilibrium calcium isotope fractionation between clinopyroxene and Ca-doped orthopyroxene. Geochim Cosmochim Acta 143:132-142
Feynman R, Hibbs A (1965) Quantum mechanics and path integrals. McGraw-Hill, New York
Fricke G, Heilig K (2004) Group I: Elementary Particles, Nuclei and Atoms. Nuclear Charge Radii (Landolt-Börnstein: Numerical Data and Functional Relationships in Science and Technology, New Series) (Springer, Berlin), Vol 20
Frisch MJ, Trucks GW, Schlegel HB, Scuseria GE, Robb MA, Cheeseman JR, Scalmani G, Barone V, Mennucci B, Petersson GA, Nakatsuji H, Caricato M, Li X, Hratchian HP, Izmaylov AF, Bloino J, Zheng G, Sonnenberg JL, Hada M, Ehara M, Toyota K, Fukuda R, Hasegawa J, Ishida M, Nakajima T, Honda Y, Kitao O, Nakai H, Vreven T, Montgomery Jr JA, Peralta JE, Ogliaro F, Bearpark M, Heyd JJ, Brothers E, Kudin KN, Staroverov VN, Kobayashi R, Normand J, Raghavachari K, Rendell A, Burant JC, Iyengar SS, Tomasi J, Cossi M, Rega N, Millam NJ, Klene M, Knox JE, Cross JB, Bakken V, Adamo C, Jaramillo J, Gomperts R, Stratmann RE, Yazyev O, Austin AJ, Cammi R, Pomelli C, Ochterski JW, Martin RL, Morokuma K, Zakrzewski VG, Voth GA, Salvador P, Dannenberg JJ, Dapprich S, Daniels AD, Farkas O, Foresman JB, Ortiz JV, Cioslowski J, Fox DJ (2009) Gaussian 09, Revision B.01, Gaussian Inc, Wallingford, CT
Fujii T, Albarède F (2012) Ab initio calculation of the Zn isotope effect in phosphates, citrates, and malates and applications to plants and soil. PLoS ONE 7:e30726
Fujii T, Moynier F, Albarède F (2006a) Nuclear field vs. nucleosynthetic effects as cause of isotopic anomalies in the early Solar System. Earth Planet Sci Lett 247:1-9
Fujii T, Moynier F, Telouk P, Albarède F (2006b) Mass-independent isotope fractionation of molybdenum and ruthenium and the origin of isotopic anomalies in Murchison. Astrophys J 647:1506-1516
Fujii T, Fukutani S, Yamana H (2008) Isotope fractionation of strontium in a precipitation reaction of SrO_2. J Nucl Sci Technol Suppl 6:15-18
Fujii T, Moynier F Albarède F (2009) The nuclear field shift effect in chemical exchange reactions. Chem Geol 267:139-156
Fujii T, Moynier F, Telouk P, Abe M (2010) Experimental and theoretical investigation of isotope fractionation of zinc between aqua, chloro, and macrocyclic complexes. J Phys Chem A 114:2543-2552
Fujii T, Moynier F, Pons M-L, Albarède F (2011) The origin of Zn isotope fractionation in sulfides. Geochim Cosmochim Acta 75:7632-7643
Fujii T, Moynier F, Abe M, Nemoto K, Albarède F (2013) Copper isotope fractionation between aqueous compounds relevant to low temperature geochemistry and biology. Geochim Cosmochim Acta 110:29-44
Fujii T, Moynier F, Agranier A, Ponzevera E, Abe M, Uehara A, Yamana H (2013) Nuclear field shift effect in isotope fractionation of thallium. J Radioanal Nucl Chem 296, 261–265
Fujii T, Moynier F, Blichert-Toft J, Albarède F (2014) Density functional theory estimation of isotope fractionation of Fe, Ni, Cu, and Zn among species relevant to geochemical and biological environments. Geochim Cosmochim Acta 140:553-576
Fujii T, Pringle EA, Chaussidon M, Moynier F (2015) Isotope fractionation of Si in protonation/deprotonation reaction of silicic acid: A new pH proxy. Geochim Cosmochim Acta 168:193-205
Gao YQ, Marcus RA (2001) Strange and unconventional isotope effects in ozone formation. Science 293:259-263

Garlick GD (1966) Oxygen isotope fractionation in igneous rocks. Earth Planet Sci Lett 1:361-368
Garrity KF, Bennett JW, Rabe KM, Vanderbilt D (2014) Pseudopotentials for high-throughput DFT calculations. Comput Mater Sci 81:446-452
Georg RB, Halliday AN, Schauble EA, Reynolds BC (2007) Silicon in the Earth's core. Nature 447:1102-1106
Ghosh S, Schauble EA, Lacrampe Couloume G, Blum JD, Bergquist BA (2013) Estimation of nuclear volume dependent fractionation of mercury isotopes in equilibrium liquid–vapor evaporation experiments. Chem Geol 336:5-12
Giannozzi P, Baroni S, Bonini N, Calandra M, Car R, Cavazzoni C, Ceresoli D, Chiarotti GL, Cococcioni M, Dabo I, Dal Corso A, de Gironcoli S, Fabris S, Fratesi G, Gebauer R, Gerstmann U, Gougoussis C, Kokalj A, Lazzeri M, Martin-Samos L, Marzari N, Mauri F, Mazzarello R, Paolini S, Pasquarello A, Paulatto L, Sbraccia C, Scandolo S, Sclauzero G, Seitsonen AP, Smogunov A, Umari P, Wentzcovitch RM (2009) Quantum ESPRESSO: a modular and open-source software project for quantum simulations of materials. J Phys Condens Matter 21:395502
Gonze X, Beuken J-M, Caracas R, Detraux F, Fuchs M, Rignanese G-M, Sindic L, Verstraete M, Zerah G, Jollet F, Torrent M, Roy A, Mikami M, Ghosez Ph, Raty J-Y, Allan DC (2002) First-principles computation of material properties : the ABINIT software project. Comput Mat Sci 25:478-492
Griffith EM, Schauble EA, Bullen TD, Paytan A (2008) Characterization of calcium isotopes in natural and synthetic barite. Geochim Cosmochim Acta 72:5641-5658
Grimme S (2011) Density functional theory with London dispersion corrections. WIREs Comput Mol Sci 1:211-228
He H, Liu Y (2015) Silicon isotope fractionation during the precipitation of quartz and the adsorption of H_4SiO_4(aq) on Fe(III)-oxyhydroxide surfaces. Chin J Geochem 34:459-468
He H, Zhang S, Zhu C, Liu Y (2016) Equilibrium and kinetic Si isotope fractionation factors and their implications for Si isotope distributions in the Earth's surface environments. Acta Geochim 35:15-24
Heidenreich JE, Thiemens MH (1986) A non-mass-dependent oxygen isotope effect in the production of ozone from molecular oxygen: the role of molecular symmetry in isotope chemistry. J Chem Phys 84 (4):2129
Hill PS, Schauble EA (2008) Modeling the effects of bond environment on equilibrium iron isotope fractionation in ferric aquo-chloro complexes. Geochim Cosmochim Acta 72:1939–1958
Hill PS, Schauble EA, Young ED (2010) Effects of changing solution chemistry on Fe^{3+}/Fe^{2+} isotope fractionation in aqueous Fe–Cl solutions. Geochim Cosmochim Acta 74:6669–6689
Hofmann MEG, Horváth B, Pack A (2012) Triple oxygen isotope equilibrium fractionation between carbon dioxide and water. Earth Planet Sci Lett 319-320:159-164
Hohenberg P, Kohn W (1964) Inhomogeneous electron gas. Phys Rev 136:B864-871
Horita J, Cole DR, Polyakov VB, Driesner T (2002) Experimental and theoretical study of pressure effects on hydrogen isotope fractionation in the system brucite-water at elevated temperatures. Geochim Cosmochim Acta 66:3769-3788
Huang F, Chen L, Wu Z, Wang W (2013) First-principles calculations of equilibrium Mg isotope fractionations between garnet, clinopyroxene, orthopyroxene, and olivine: Implications for Mg isotope thermometry. Earth Planet Sci Lett 367:61-70
Huang F, Wu Z, Huang S, Wu F (2014) First-principles calculations of equilibrium silicon isotope fractionation among mantle minerals. Geochim Cosmochim Acta 140:509-520
Hulston JR, Thode HG (1965) Variations in the S^{33}, S^{34}, and S^{36} contents of meteorites and their relation to chemical and nuclear effects, J Geophys Res 70:3475–3484
Ishida T (2002) Isotope effect and isotopic separation: A chemist's view. Journal of nuclear science and technology 39:407-412

Jahn S, Wunder B (2009) Lithium speciation in aqueous fluids at high P and T studied by ab initio molecular dynamics and consequences for Li-isotope fractionation between minerals and fluids. Geochim Cosmochim Acta 73:5428-5434

Jancso G, Rebelo LPN, Van Hook WA (1993) Isotope effects in solution thermodynamics: Excess properties in solutions of isotopomers. Chem Rev 93:2645-2666

Javoy M, Balan E, Méheut M, Blanchard M, Lazzeri M (2012) First-principles investigation of equilibrium isotopic fractionation of O- and Si-isotopes between refractory solids and gases in the solar nebula. Earth Planet Sci Lett 319/320:118-127

Kieffer SW (1982) Thermodynamics and lattice vibrations of minerals: 5. Applications to phase equilibria, isotopic fractionation, and high-pressure thermodynamic properties. Rev Geophys Space Phys 20:827-849

King WH (1984) Isotope shifts in atomic spectra. Plenum Press, New York.

Kleinman LI, Wolfsberg M (1973) Corrections to the Born-Oppenheimer approximation and electronic effects on isotopic exchange equilibria. J Chem Phys 59:2043-2053

Klochko K, Kaufman AJ, Yao W, Byrne RH, Tossell JA (2006) Experimental measurement of boron isotope fractionation in seawater. Earth Planet Sci Lett 248:276-285

Knyazev DA, Myasoedov NF (2001) Specific effects of heavy nuclei in chemical equilibirum. Separation Sci Technol 36:1677-1696

Knyazev DA, Semin GK, Bochkarev AV (1999) Nuclear quadrupole contribution to the equilibrium isotope effect. Polyhedron 18:2579-2582

Kohn W, Sham LJ (1965) Self-consistent equations including exchange and correlation effects. Phys Rev 140:A1133-A1138

Kowalski PM, Jahn S (2011) Prediction of equilibrium Li isotope fractionation between minerals and aqueous solutions at high P and T: An efficient ab initio approach. Geochim Cosmochim Acta 75:6112-6123

Kowalski PM, Wunder B, Jahn S (2013) Ab-initio prediction of equilibrium boron isotope fractionation between minerals and aqueous fluids at high P and T. Geochim Cosmochim Acta 101:285-301

Kresse G, Furthmüller J (1996) Efficient iterative schemes for ab initio total-energy calculations using a plane wave basis set. Phys Rev B 54:11169–11186

Landau L, Lifshitz E (1980) Course of Theoretical Physics. Statistical Physics. Part 1. Pergamon 5

Lee C, Yang W, Parr RG (1988) Development of the Colle-Salvetti correlation-energy formula into a functional of the electron density. Phys Rev B 37:785-789

Li X, Zhao H, Tang M, Liu Y (2009) Theoretical prediction for several important equilibrium Ge isotope fractionation factors and geological implications. Earth Planet Sci Lett 287:1-11

Li XF, Liu Y (2010) First-principles study of Ge isotope fractionation during adsorption onto Fe(III)-oxyhydroxide surfaces. Chem Geol 278:15-22

Li XF, Liu Y (2011) Equilibrium Se isotope fractionation parameters: A first-principles study. Earth Planet Sci Lett 304:113-120

Liu Y, Tossell JA (2005) Ab initio molecular orbital calculations for boron isotope fractionations on boric acids and borate. Geochim Cosmochim Acta 69, 3995-4006

Liu Q, Tossell JA, Liu Y (2010) On the proper use of the Bigeleisen-Mayer equation and corrections to it in the calculation of isotopic fractionation equilibrium constants. Geochim Cosmochim Acta 74:6965-6983

Lyons JR, Young ED (2005) CO self-shielding as the origin of oxygen isotope anomalies in the early solar nebula. Nature 435:317-320

Lyons JR (2007) Mass-independent fractionation of sulfur isotopes by isotope-selective dissociation of SO_2. Geophys Res Lett 34:L22811

Markland TE, Berne B (2012) Unraveling quantum mechanical effects in water using isotopic fractionation. Proc Natl Acad Sci USA 109:7988–7991

Marsalek O, Chen P-Y, Dupuis R, Benoit M, Méheut M, Bacic Z, Tuckerman ME (2014) Efficient calculation of free energy differences associated with isotopic substitution using

path-integral molecular dynamics. J Chem Theory Comput 10:1440-1453
Marx D, Hutter J (2000) Ab initio molecular dynamics: theory and implementation. In Modern Methods and Algorithms of Quantum Chemistry, vol. 1 (ed. J. Grotendorst). NIC, FZ Jülich, pp. 301–449; CPMD Code: J. Hutter et al. Available from: www.cpmd.org/
Matsuhisa Y, Goldsmith JR, Clayton RN (1978) Mechanisms of hydrothermal crystallization of quartz at 250ºC and 15 kbar. Geochim Cosmochim Acta 42:173-182
Mauersberger K (1987) Ozone isotope measurements in the stratosphere. Geophys Res Lett 14:80-83
Méheut M, Lazzeri M, Balan E, Mauri F (2007) Equilibrium isotopic fractionation between kaolinite, quartz and water: prediction from first-principles density functional theory. Geochim Cosmochim Acta 71:3170-3181
Méheut M, Lazzeri M, Balan E, Mauri F (2009) Structural control over equilibrium silicon and oxygen isotopic fractionation: a first-principles density-functional theory study. Chem Geol 258:28-37
Méheut M, Schauble EA (2014) Silicon isotope fractionation in silicate minerals: Insights from first-principles models of phyllosilicates, albite and pyrope. Geochim Cosmochim Acta 134:137-154
Mielke SL, Truhlar DG (2009) Improved methods for Feynman path integral calculations of vibrational-rotational free energies and application to isotopic fractionation of hydrated chloride ions. J Phys Chem A 113:4817-4827
Miller CA, Peucker-Ehrenbrink B, Schauble EA (2015) Theoretical modelling of rhenium isotope fractionation, natural variations across a black shale weathering profile, and potential as a paleoredox proxy. Earth Planet Sci Lett 430:339-348
Mook WG (2000) Environmental Isotopes in the Hydrological Cycle Principles and Applications, V, I: Introduction–Theory, Methods, Review. UNESCO/IAEA, Geneva.
Moynier F, Yin Q-Z, Schauble E (2011) Isotopic evidence of Cr partitioning into Earth's core. Science 331:1417-1420
Moynier F, Fujii T, Wang K, Foriel J (2013) Ab initio calculations of the Fe(II) and Fe(III) isotopic effects in citrates, nicotianamine, and phytosiderophore, and new Fe isotopic measurements in higher plants. Comptes Rendus Géoscience 245:230-240
Nadjakov EG, Marinova KP, Gangrsky YuP (1994) Systematics of nuclear charge radii. At Data Nucl Data Tables 56:133-157
Nemoto K, Abe M, Seino J, Hada M (2015) An ab initio study of nuclear volume effects for isotope fractionations using two-component relativistic methods. J Comput Chem 36:816-820
Nishizawa K, Satoyama T, Miki T, Yamamoto T, Hosoe M (1995) Strontium isotope effect in liquid-liquid extraction of strontium chloride using a crown ether. J. Nucl. Sci. Technol 32:1230-1235
Nomura M, Higuchi N, Fujii Y (1996) Mass dependence of uranium isotope effects in the U(IV)−U(VI) exchange reaction. J Am Chem Soc 118:9127–9130
Otake T, Lasaga AC, Ohmoto H (2008) Ab initio calculations for equilibrium fractionations in multiple sulfur isotope systems. Chem Geol 249:357-376.
Ottonello G, Zuccolini MV (2005) Ab-initio structure, energy and stable Cr isotopes equilibrium fractionation of some geochemically relevant H-O-Cr-Cl complexes. Geochim Cosmochim Acta 69:851-874
Ottonello G, Zuccolini MV (2008) The iron-isotope fractionation dictated by the carboxylic functional: An ab-initio investigation. Geochim Cosmochim Acta 72:5920-5934
Ottonello G, Zuccolini MV (2009) Ab-initio structure, energy and stable Fe isotope equilibrium fractionation of some geochemically relevant H–O–Fe complexes. Geochim Cosmochim Acta 73:6447-6469
Ottonello G, Civalleri B, Zuccolini MV, Zicovich-Wilson (2007) Ab-initio thermal physics and Cr-isotopic fractionation of $MgCr_2O_4$. Am Mineral 92:98-108
Pavlov AA, Kasting JF (2002) Mass-independent fractionation of sulfur isotopes in Archean

sediments: Strong evidence for an anoxic Archean atmosphere: Astrobiology, 2:27-41
Pérez A, von Lilienfeld OA (2011) Path integral computation of quantum free energy differences due to alchemical transformations involving mass and potential. J Chem Theory Comput 7:2358-2369
Perdew JP, Ruzsinszky A (2010) Density functional theory of electronic structure: A short course for mineralogists and geophysicists. Rev Mineral Geochem 71:1-18
Pinilla C, Blanchard M, Balan E, Ferlat G, Vuilleumier R, Mauri F (2014) Equilibrium fractionation of H and O isotopes in water from path integral molecular dynamics. Geochim Cosmochim Acta 135:203-216
Pinilla C, Blanchard M, Balan E, Natarajan SK, Vuilleumier R, Mauri F (2015) Equilibrium magnesium isotope fractionation between aqueous Mg^{2+} and carbonate minerals: insights from path integral molecular dynamics. Geochim Cosmochim Acta 163:126-139
Polyakov VB (1997) Equilibrium fractionation of the iron isotopes: Estimation from Mössbauer spectroscopy data. Geochim Cosmochim Acta 61:4213-4217
Polyakov VB, Mineev SD (2000) The use of Mössbauer spectroscopy in stable isotope geochemistry. Geochim Cosmochim Acta 64:849-865
Polyakov VB, Mineev SD, Clayton RN, Hu G, Mineev KS (2005) Determination of tin equilibrium isotope fractionation factors from synchrotron radiation experiments. Geochim Cosmochim Acta 69:5531-5536
Polyakov VB, Clayton RN, Horita J, Mineev SD (2007) Equilibrium iron isotope fractionation factors of minerals: reevaluation from the data of nuclear inelastic resonant X-ray scattering and Mössbauer spectroscopy. Geochim Cosmochim Acta 71:3833-3846
Polyakov VB, Soultanov DM (2011) New data on equilibrium iron isotope fractionation among sulfides: constraints on mechanisms of sulfide formation in hydrothermal and igneous systems. Geochim Cosmochim Acta 75:1957-1974
Polyakov V, Osadchii E, Chareev D, Chumakov A, Sergeev I (2013) Fe β-Factors for sulfides from NRIXS Synchrotron Experiments. Mineral Mag 77:1985
Ramírez R, Herrero CP (2010) Quantum path integral simulation of isotope effects in the melting temperature of ice Ih. J Chem Phys 133:144511
Redlich O (1935) Eine allgemeine beziehung zwischen den schwingungsfrequenzen isotoper molekeln. Z Phys Chem B 28:371-382
Rehkämper M, Frank M, Hein JR, Porcelli D, Halliday A, Ingri J, Liebetrau V (2002) Thallium isotope variations in seawater and hydrogenetic, diagenetic, and hydrothermal ferromanganese deposits. Earth Planet Sci Lett 197:65-81
Richet P, Bottinga Y, Javoy M (1977) A review of hydrogen, carbon, nitrogen, oxygen, sulphur, and chlorine stable isotope fractionation among gaseous molecules. Ann Rev Earth Planet Sci 5:65-110
Richter R, Hoernes S (1988) The application of the increment method in comparison with experimentally derived and calculated O-isotope fractionations. Chem Erde 48:1-18
Roothaan CCJ (1951) New developments in molecular orbital theory. Rev Modern Phys 23:69-89
Roskosz M, Sio CKI, Dauphas N, Bi W, Tissot FHL, Hu MY, Zhao J, Alp EE (2015) Spinel-olivine-pyroxene equilibrium iron isotopic fractionation and applications to natural peridotites. Geochim Cosmochim Acta 169:184-199
Rumble D, Miller MF, Franchi IA, Greenwood RC (2007) Oxygen three-isotope fractionation lines in terrestrial silicate minerals: an inter-laboratory comparison of hydrothermal quartz and eclogitic garnet Geochim Cosmochim Acta 71:3592–3600
Rustad JR, Bylaska EJ (2007) Ab initio calculation of isotopic fractionation in $B(OH)_3$(aq) and $B(OH)_4^-$(aq). J Am Chem Soc 129:2222–2223
Rustad JR, Dixon DA (2009) Prediction of iron-isotope fractionation between hematite (α-Fe_2O_3) and ferric and ferrous iron in aqueous solution from density functional theory. J Phys Chem A 113:12249-12255
Rustad JR, Yin Q-Z (2009) Iron isotope fractionation in the Earth's lower mantle. Nature

Geoscience 2:514-518
Rustad JR, Casey WH, Yin Q-Z, Bylaska EJ, Felmy AR, Bogatko SA, Jackson VE, Dixon DA (2010) Isotopic fractionation of Mg^{2+}, Ca^{2+}, and Fe^{2+} with carbonate minerals. Geochim Cosmochim Acta 74:6301-6323
Rustad JR, Bylaska EJ, Jackson VE, Dixon DA (2010) Calculation of boron-isotope fractionation between $B(OH)_3$(aq) and $B(OH)_4^-$(aq). Geochim Cosmochim Acta 74:2843-2850
Schauble EA (2004) Applying stable isotope fractionation theory to new systems. Rev Mineral Geochem 55:65-111
Schauble EA (2007) Role of nuclear volume in driving equilibrium stable isotope fractionation of mercury, thallium, and other very heavy elements. Geochim Cosmochim Acta 71:2170-2189
Schauble EA (2011) First-principles estimates of equilibrium magnesium isotope fractionation in silicate, oxide, carbonate and hexaaquamagnesium(2+) crystals. Geochim Cosmochim Acta 75:844-869
Schauble EA, Rossman GR, Taylor HP Jr (2004) Theoretical estimates of equilibrium chromium-isotope fractionations, Chem Geol 205:99-114
Schauble EA, Ghosh P, Eiler JM (2006) Preferential formation of ^{13}C-^{18}O bonds in carbonate minerals, estimated using first-principles lattice dynamics. Geochim Cosmochim Acta 70:2510-2529
Schauble EA (2013) Modeling nuclear volume isotope effects in crystals. Proc Nat Acad Sci (USA) 110:17714-17719
Schmidt MW, Baldridge KK, Boatz JA, Elbert ST, Gordon MS, Jensen JH, Koseki S, Matsunaga N, Nguyen KA, Su S, Windus TL, Dupuis M, Montgomery JA (1993) General Atomic and Molecular Electronic Structure System. J Comput Chem 14:1347-1363
Schott J, Mavromatis V, Fujii T, Pearce CR, Oelkers EH (2016) The control of magnesium aqueous speciation on Mg isotope composition in carbonate minerals: Theoretical and experimental modeling. Chem Geol doi: 10.1016/j.chemgeo.2016.03.011
Schütze H (1980) Der Isotopenindex-eine Inkrementenmethode zur näherungsweise Berechnung von Isotopenaustauschgleichgewichten zwischen kristallinen Substanzen. Chem Erde 39:321-334
Schuchardt KL, Didier BT, Elsethagen T, Sun L, Gurumoorthi V, Chase J, Li J, Windus TL (2007) Basis Set Exchange: A Community Database for Computational Sciences. J Chem Inf Model 47:1045-1052
Seo JH, Lee SK, Lee I (2007) Quantum chemical calculations of equilibrium copper (I) isotope fractionations in ore-forming fluids. Chem Geol 243:225-237
Sherman DM (2013) Equilibrium isotopic fractionation of copper during oxidation/reduction, aqueous complexation and ore-forming processes: Predictions from hybrid density functional theory. Geochim Cosmochim Acta 118, 85-97
Skulan JL, Beard BL, Johnson CM (2002) Kinetic and equilibrium Fe isotope fractionation between aqueous Fe(III) and hematite. Geochim Cosmochim Acta 66:2995-3015
Smyth JR, Clayton RN (1988) Correlation of oxygen isotope fractionation and electrostatic site potentials in silicates. Eos 69:1514 (abstr.)
Stillinger FH, Weber TA (1983) Inherent structure in water. J Phys Chem 87:2833–2840
Stirling CH, Andersen MB, Potter E-K, Halliday AN (2007) Low-temperature isotopic fractionation of uranium. Earth Planet Sci Lett 264:208-225
Suzuki K, Shiga M, Tachikawa M (2008) Temperature and isotope effects on water cluster ions with path integral molecular dynamics based on the forth order Trotter expansion. J Chem Phys 129:144310
Syverson DD, Borrok DM, Seyfried Jr WE (2013) Experimental determination of equilibrium Fe isotopic fractionation between pyrite and dissolved Fe under hydrothermal conditions. Geochim Cosmochim Acta 122:170-183
Tachikawa M, Shiga M (2005) Ab initio path integral simulation study on $^{16}O/^{18}O$ isotope effect in water and hydronium ion. Chem Phys Lett 407:135-138

Taylor HP Jr, Epstein S (1962) Relationships between $^{18}O/^{16}O$ ratios in coexisting minerals of igneous and metamorphic rocks, Part 2. Application to petrologic problems. G S A Bull 73:675-694
Tossell JA (2005) Calculating the partitioning of the isotopes of Mo between oxidic and sulfidic species in aqueous solution. Geochim Cosmochim Acta 69:2981-2993
Tossell JA (2006) Boric acid adsorption on humic acids: Ab initio calculation of structures, stabilities, B-11 NMR and B-11, B-10 isotopic fractionations of surface complexes. Geochim Cosmochim Acta 70:5089-5103
Tuckerman M (2010) Statistical mechanics: theory and molecular simulation. Oxford University Press
Tuckerman ME, Yarne DA, Samuelson SO, Hughes AL, Martyna GJ (2000) Exploiting multiple levels of parallelism in molecular dynamics based calculations via modern techniques and software paradigms on distributed memory computers. Comp Phys Commun 128:333–376
Turro NJ (1983) Influence of nuclear spin on chemical reactions: Magnetic isotope and magnetic field effects (a review). Proc Natl Acad Sci USA 80:609-621
Urey HC (1947) The thermodynamic properties of isotopic substances. J Chem Soc (Lond.) 562-581
Valiev M, Bylaska EJ, Govind N, Kowalski K, Straatsma TP, van Dam HJJ, Wang D, Nieplocha J, Apra E, Windus TL, de Jong WA (2010) NWChem: a comprehensive and scalable open-source solution for large scale molecular simulations. Comput Phys Commun 181:1477
Vanicek J, Miller W (2007) Efficient estimators for quantum instanton evaluation of the kinetic isotope effects: application to the intramolecular hydrogen transfer in pentadiene. J Chem Phys 127:114309
Wasylenki LE, Rolfe BA, Weeks CL, Spiro TG, Anbar AD (2008) Experimental investigation of the effects of temperature and ionic strength on Mo isotopic fractionation during adsorption to manganese oxide. Geochim Cosmochim Acta 72:5997-6005
Wasylenki LE, Weeks CL, Bargar JR, Spiro TG, Hein JR, Anbar AD (2011) The molecular mechanism of Mo isotope fractionation during adsorption to birnessite. Geochim Cosmochim Acta 75, 5019-5031
Webb MA, Miller TF (2014) Position-specific and clumped stable isotope studies: comparison of the Urey and path-integral approaches for carbon dioxide, nitrous oxide, methane, and propane. J Phys Chem A 118:467-474
Weeks CL, Anbar AD, Wasylenki LE, Spiro TG (2007) Density functional theory analysis of molybdenum isotope fractionation. J Phys Chem A 111:12434-12438
Weeks CL, Anbar AD, Wasylenki LE, Spiro TG (2008) Density functional theory analysis of molybdenum isotope fractionation (correction to v111, 12434, 2007). J Phys Chem A 112:10703
Welch SA, Beard BL, Johnson CM, Braterman PS (2003) Kinetic and equilibrium Fe isotope fractionation between aqueous Fe(II) and Fe(III). Geochim Cosmochim Acta 67:4231–4250
Weston RE Jr. (1999) Anomalous or mass-independent isotope effects. Chem Rev 99:2115-2136
Widanagamage IH, Schauble EA, Scher HD, Griffith EM (2014) Stable strontium isotope fractionation in synthetic barite. Geochim Cosmochim Acta 147:58-75
Wiederhold JG, Cramer CJ, Daniel K, Infante I, Bourdon B, Kretzschmar R (2010) Equilibrium mercury isotope fractionation between dissolved Hg(II) species and thiol-bound Hg. Environ Sci Technol 44:4191-4197
Wiesli RA, Beard BL, Johnson CM (2004) Experimental determination of Fe isotope fractionation between aqueous Fe(II), siderite and “green rust” in abiotic systems. Chem Geol 211:343-362
Wilson EBJ, Decius JC, Cross PC (1955) Molecular Vibrations: The Theory of Infrared and Raman Vibrational Spectra. Dover, New York
Wu F, Qin T, Li X, Liu Y, Huang J-H, Wu Z, Huang F (2015) First-principles investigation of vanadium isotope fractionation in solution and during adsorption. Earth Planet Sci Lett

426:216-224
Wu ZQ, Huang F, Huang S (2015) Isotope fractionation induced by phase transformation: First-principles investigation for Mg2SiO4. Earth Planet Sci Lett 409:339-347
Yamaji K, Makita Y, Watanabe H, Sonoda A, Kanoh H, Hirotsu T, Ooi K (2001) Theoretical estimation of lithium isotopic reduced partition function ratio for lithium ions in aqueous solution. J Phys Chem A 105:602–613
Yang S, Liu Y (2015) Nuclear volume effects in equilibrium stable isotope fractionations of mercury, thallium and lead. Sci Reports 5:12626
Yang JL, Li YB, Liu SQ, Tian HQ, Chen CY, Liu JM, Shi YL (2015) Theoretical calculations of Cd isotope fractionation in hydrothermal fluids. Chem Geol 391:74-82
Young ED, Galy A, Nagahara H (2002) Kinetic and equilibrium mass-dependent isotope fractionation laws in nature and their geochemical and cosmochemical significance. Geochim Cosmochim Acta 66:1095–1104
Young ED, Manning CE, Schauble EA, Shahar A, Macris CA, Lazar C, Jordan M (2015) High-temperature equilibrium isotope fractionation of non-traditional stable isotopes : Experiments, theory, and applications. Chem Geology 395:176-195
Zeebe RE (2005) Stable boron isotope fractionation between dissolved $B(OH)_3$ and $B(OH)_4^-$. Geochim Cosmochim Acta 69:2753-2766
Zeidler A, Salmon PS, Fischer HE, Neuefeind JC, Simonson JM, Markland TE (2012) Isotope effects in water as investigated by neutron diffraction and path integral molecular dynamics. J Phys: Condens Matter 24:284126
Ziegler K, Young ED, Schauble EA, Wasson JT (2010) Metal-silicate silicon isotope fractionation in enstatite meteorites and constraints on Earth's core formation. Earth Planet Sci Lett 295:487-496
Zwanziger J (2009) Computation of Mössbauer isomer shifts from first principles. J Phys Condens Matter 21:195501